scientific reports

Check for updates

OPEN

C. elegans PPEF-type phosphatase (Retinal degeneration C ortholog) functions in diverse classes of cilia to regulate nematode behaviors

Marine Barbelanne[1,2], Yun Lu[3], Keerthana Kumar[1,2], Xinxing Zhang[4], Chunmei Li[1,2], Kwangjin Park[1,2], Adam Warner[1,2], X. Z. Shawn Xu[4], Shai Shaham[3] & Michel R. Leroux[1,2]✉

Primary (non-motile) cilia represent structurally and functionally diverse organelles whose roles as specialized cellular antenna are central to animal cell signaling pathways, sensory physiology and development. An ever-growing number of ciliary proteins, including those found in vertebrate photoreceptors, have been uncovered and linked to human disorders termed ciliopathies. Here, we demonstrate that an evolutionarily-conserved PPEF-family serine-threonine phosphatase, not functionally linked to cilia in any organism but associated with rhabdomeric (non-ciliary) photoreceptor degeneration in the *Drosophila* rdgC (retinal degeneration C) mutant, is a *bona fide* ciliary protein in *C. elegans*. The nematode protein, PEF-1, depends on transition zone proteins, which make up a 'ciliary gate' in the proximal-most region of the cilium, for its compartmentalization within cilia. Animals lacking PEF-1 protein function display structural defects to several types of cilia, including potential degeneration of microtubules. They also exhibit anomalies to cilium-dependent behaviors, including impaired responses to chemical, temperature, light, and noxious CO_2 stimuli. Lastly, we demonstrate that PEF-1 function depends on conserved myristoylation and palmitoylation signals. Collectively, our findings broaden the role of PPEF proteins to include cilia, and suggest that the poorly-characterized mammalian PPEF1 and PPEF2 orthologs may also have ciliary functions and thus represent ciliopathy candidates.

Keywords Cilia, PPEF, Phosphatase, PEF-1, Behavior, Chemosensation, Thermosensation, Photosensation, CO2, *C. elegans*

Primary cilia are complex cellular organelles found across a diverse range of cell types in metazoans[1–4]. They act as specialized antenna, harboring receptors and signal transduction proteins finely tuned to capture and propagate distinct environmental signals[5,6]. Such compartmentalization of the signaling machinery allows cilia to orchestrate various cell signaling pathways and play essential roles in physiology and development. For example, in humans, olfactory cilia enable olfaction (smell), neuronal cilia relay hormonal (such as satiety) signals, and rod/cone ciliary photoreceptors transduce visual information[7–11]. Defects in the formation or function of primary cilia result in so-called ciliopathies that collectively affect most organs[12,13]. Nearly 200 genes are implicated in such disorders, whose clinical phenotypes include but is not limited to retinal degeneration, cystic kidneys, obesity, congenital heart defects, as well as skeletal and brain malformations[13–18].

Cilia are anchored at the plasma membrane by a modified centriole termed basal body[19,20]. The ciliary backbone, or axoneme, is enveloped by a distinctive ciliary membrane contiguous with the cell body membrane[21]. In most cell types, the axoneme is built using a conserved kinesin- and dynein-driven intraflagellar transport (IFT) system, and consists of nine concentric doublet microtubules with a distal region composed of singlet microtubules[22–24]. Within the most proximal region of the axoneme is a conserved subdomain, the transition zone, which functions as a selective diffusion barrier ('ciliary gate') that regulates the composition of the ciliary compartment[25–27]. Most primary cilia are unitary and rod- or whip-shaped, but depending on the organism

[1]Department of Molecular Biology and Biochemistry, Simon Fraser University, 8888 University Drive, Burnaby, BC V5A 1S6, Canada. [2]Centre for Cell Biology, Development, and Disease, Simon Fraser University, 8888 University Drive, Burnaby, BC V5A 1S6, Canada. [3]Laboratory of Developmental Genetics, The Rockefeller University, 1230 York Avenue, New York, NY 10065, USA. [4]Life Sciences Institute, Department of Molecular and Integrative Physiology, University of Michigan, Ann Arbor, MI 48109, USA. ✉email: leroux@sfu.ca

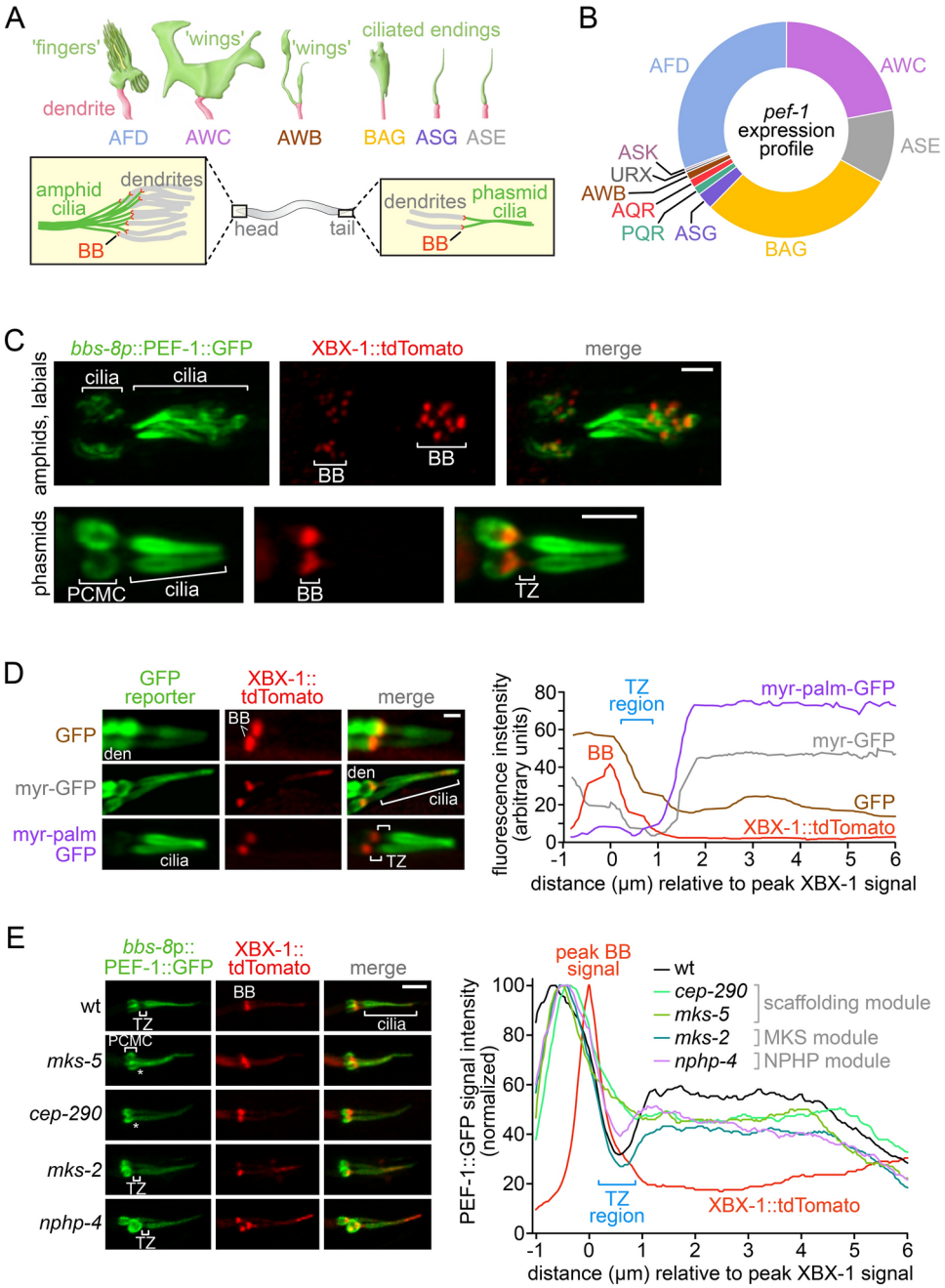

and cell type, substantial variations exist[28]. For instance, mammalian olfactory neurons contain multiple long cilia[29,30], some ependymal cells are bi-ciliated[31], and photoreceptor ciliary outer segments (distal to the transition zone) comprise a complex array of membrane folds that house rhodopsin, the light-sensing G protein-coupled receptor (GPCR)[8,9,32,33].

The nematode *C. elegans* has proven to be a useful model system to identify novel cilium-associated proteins and dissect their roles in cilium formation and function. Its cilia are exclusively non-motile and found within sensory neurons at the distal ends of dendrites[34–36]. The cilia exhibit an assortment of shapes (Fig. 1A), with each ciliary type specifically adapted for their particular sensory functions[37]. For instance, rod-like and bi-ciliated cilia (*e.g.*, from ASE/ADL/ASH neurons) perform roles in chemosensation, osmosensation, photosensation and/or mechanosensation; 'wing'- and 'bag'-shaped cilia (AWA/AWB/AWC/BAG neurons) sense volatile odorants and gases, including oxygen and carbon dioxide; lastly, an elaborate ciliary compartment containing numerous microvilli (AFD neuron) acts as a highly sensitive thermosensor[34,35,37–40].

Using available *C. elegans* single-cell transcriptome data to enrich for genes specifically expressed in ciliated cells, we identified PEF-1, a member of the evolutionarily-conserved serine-threonine PPEF phosphatase family[41], as a strong candidate for having a ciliary function. Currently no PPEF family member has been functionally linked to cilia, although notably, the *C. elegans* ortholog, PEF-1, was shown in 2001 by Ramulu and Nathans to be localized to the distal ends of dendrites, presumably within cilia, and that this localization depends on an N-terminal myristoylation and palmitoylation concensus sequence (MGCxxS/T)[42]. We demonstrate that

◀**Fig. 1**. The myristoylated and palmitoylated serine-threonine phosphatase PPEF *C. elegans* ortholog, PEF-1, is compartmentalized within cilia in a transition zone-dependent manner. (**A**). Schematics for different types of *C. elegans* ciliary structures (green) found at the ends of dendrites (pink) in sensory neurons (AFD, AWC, AWB, BAG, ASG and ASE are shown) in the head and tail of the animal. The AFD neuron 'fingers' (microvilli) are depicted green and the cilium yellow. BB, basal body. (**B**). Donut chart displaying the relative expression levels of *pef-1* in the indicated ciliated sensory neurons (based on single-cell expression profiling data in Taylor and colleagues [52]). (**C**). Representative images of wild-type worms showing the ciliary localization of PEF-1::GFP expressed from a *bbs-8* promoter construct within head neurons (amphid and labials) and tail neurons (phasmids). tdTomato-tagged XBX-1 (red) marks basal bodies (BB) strongly and ciliary axonemes more weakly. PCMC, periciliary membrane compartment; TZ, transition zone ('ciliary gate'). Scale bars, 2 µm. (**D**). Myristoylation and palmitoylation motifs in the C-terminal region of PEF-1 are sufficient to enrich a non-ciliary protein (GFP) within the ciliary compartment (the reporter is specifically expressed in phasmid neurons). GFP diffuses throughout the sensory neuron, including cilium. A myristoylated form of GFP (myr-GFP) is similarly distributed throughout the sensory neuron. A myristoylated and palmitoylated form of GFP (myr-palm-GFP) is targeted specifically to the ciliary axoneme and largely excluded from the transition zone (TZ). Representative images are shown and the distribution of each protein relative to the basal body marker (XBX-1::tdTomato) is quantitated in the graph. Scale bar, 2 µm. (**E**). The TZ 'ciliary gate' is required for the correct ciliary compartmentalization of PEF-1. In wild-type animals, PEF-1::GFP is largely excluded from the TZ and enriched in the ciliary axoneme. Loss of scaffolding modules (MKS-5 or CEP-290) leads to a redistribution of PEF-1::GFP to the TZ and outside of the cilium in the periciliary membrane compartment (PCMC). The core MKS module protein MKS-2 and core NPHP module protein NPHP-4 do not significantly influence PEF-1::GFP redistribution to the TZ. Scale bar, 4 µm.

the lipidated *C. elegans* PEF-1 protein is enriched within the ciliary axoneme, and that this requires a functionally intact transition zone 'ciliary gate'. We show that PEF-1 is required for the correct formation and/or maintenance of structurally distinct ciliary structures, and that it regulates several cilium-dependent behaviors. Finally, mutant analysis demonstrates that PEF-1 function depends on its ability to be myristoylated and palmitoylated. In sum, our work reveals an important role for *C. elegans* PEF-1 in supporting the structures and functions of several classes of cilia, a first for this family of phosphatases.

Results

Myristoylated and palmitoylated *C. elegans* PEF-1 localizes to the axonemal region of cilia

To identify novel cilium-associated proteins, we and others have employed various approaches, including comparative genomics, genetics, transcriptomics and proteomics. *C. elegans* sports 26 types of ciliated sensory neurons mostly in its head and tail (Fig. 1A), encompassing 62 out of a total of 302 neurons in adult hermaphrodites[34,35,43]. Using data from *C. elegans* single-cell transcriptomes[44], we obtained a ranked list of genes conserved in humans and preferentially expressed in ciliated sensory neurons (Suppl. Table 1). As expected, most highly-ranked genes encode proteins with established ciliary functions (77 of the top 120), including many involved in intraflagellar transport, the transition zone ('ciliary gate') and signal transduction (*e.g.*, cGMP and calcium signaling).

From the remaining candidates, we chose to characterize PEF-1 (ranked 72nd), the sole *C. elegans* member of the evolutionarily-conserved PPEF phosphatase family (Suppl. Table 1; Suppl. Figure 1) for several reasons. First, PPEF proteins have not been specifically associated with a ciliary function in any organism. Second, *C. elegans* PEF-1 is not functionally characterized (no mutants were available), but significantly, was shown to be lipidated and localized to the distal ends of some dendrites, presumably within cilia[42]. Third, the *Drosophila* PPEF ortholog, RDGC, regulates rhodopsin phosphorylation, and its disruption results in the degeneration of rhabdomeric (non-ciliary) photoreceptors[45–47]. This latter observation is interesting, as vertebrate photoreceptors harbor specialized cilia, and some invertebrate (including nematode) light-sensing neurons are also ciliated[48–50]. Finally, vertebrate PPEF proteins PPEF1 and PPEF2 are poorly studied and not currently implicated in cilium-associated (including ciliary photoreceptor) functions[51].

As a first step in characterizing the potential role of PEF-1 in cilia, we sought to corroborate the expression profile of the *pef-1* gene in ciliated sensory neurons and use an established ciliary co-marker to unambiguously assess the subcellular localization of the protein using superresolution microscopy. We generated a strain bearing a PEF-1::GFP fusion protein construct under the control of the endogenous *pef-1* promoter and observed expression in several head-localized ciliated neurons, including AFD, AWC, ASE, BAG, and PQR, as well as the tail-localized ciliated neurons PHA and PHB (Suppl. Figure 2). A CRISPR-Cas9 GFP knock-in similarly revealed the presence of PEF-1 in head- and tail-localized cilia (Suppl. Figure 2A, B). This expression profile is consistent with a recently-published single-cell resolution neuronal expression profiling (transcriptomics) study[52] (Fig. 1B) and the previously-published GFP reporter expression analysis[42].

Because endogenous expression of PEF-1 is most prevalent—yet mostly diffuse—within the large membrane regions of wing-type cilia, and weakly expressed in rod-shaped cilia, we struggled to use endogenous PEF-1 as a reliable reporter for our subsequent localization studies of the phosphatase (including the role of myristoylation and palmitoylation). We therefore used the *bbs-8* promoter to drive robust expression of the transgene in ciliated sensory neurons[53]. By employing a tdTomato-tagged IFT protein (XBX-1) protein as co-marker, we found the PEF-1::GFP protein to be concentrated within the cilium, but in a region distal to the transition zone (TZ), which represents the proximal-most region of the axoneme (Fig. 1C). Notably, the PEF-1::GFP protein was also

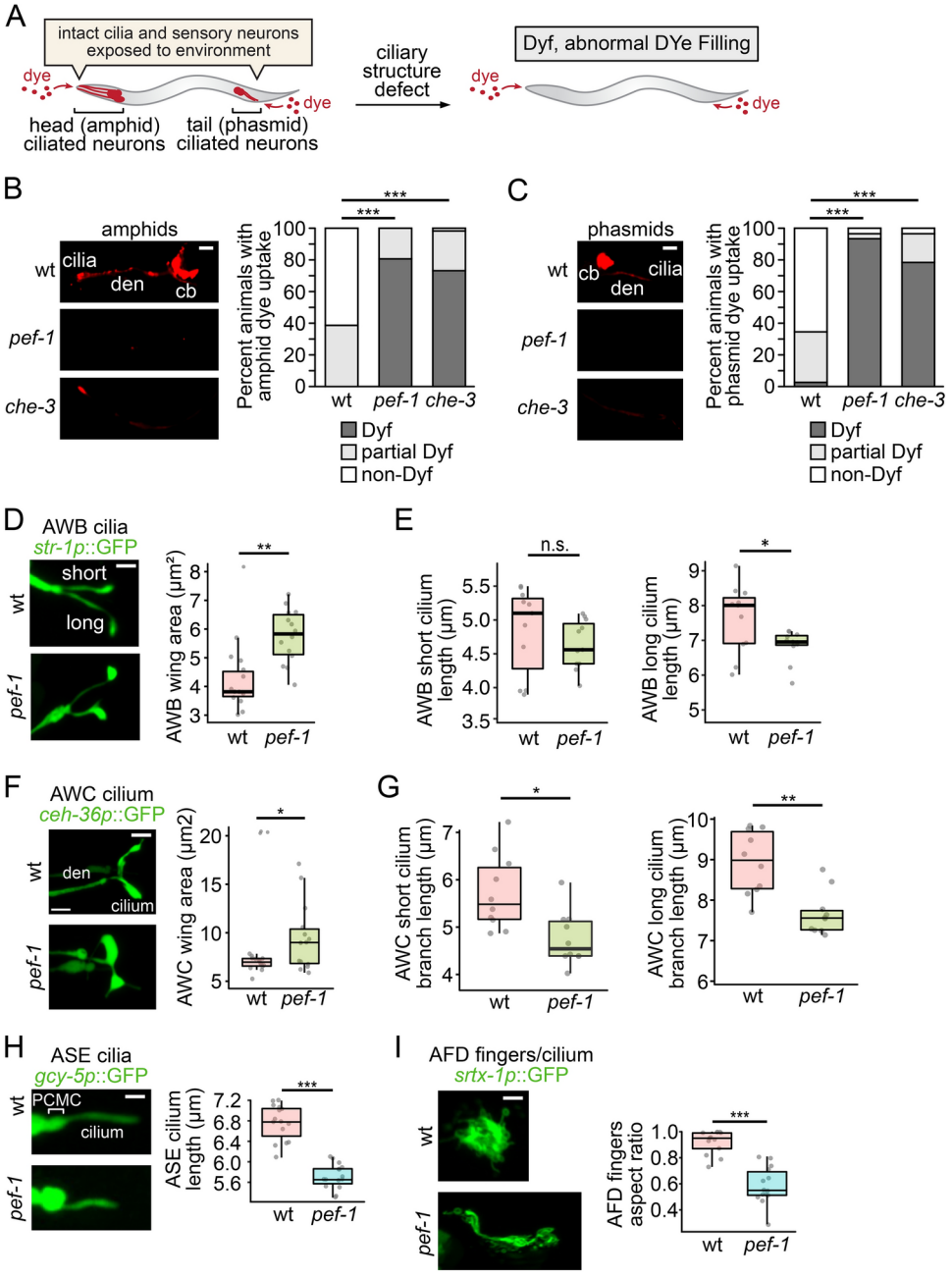

present within the periciliary membrane compartment (PCMC), at the distal end of the dendrite, where the basal body (BB) is also located (marked by XBX-1::td-Tomato; Fig. 1C).

The specific ciliary localization of PEF-1 is a property of its myristoylation and palmitoylation modifications (Suppl. Figure 2C and ref [42].). The *C. elegans* PEF-1 amino acid sequence begins with MGCGPS, which matches a well-known consensus sequence (MGCxxS/T) for myristoylation (at the glycine [G] residue) and palmitoylation (cysteine [C] residue) of various proteins, including Src family kinases and G subunits[54–56]. Palmitoylation in this context depends on the addition of a myristoyl group, and the lipid modifications work together to ensure stronger membrane association[54]. Hence, a G2A mutation inhibits both modifications, while a C3S disrupts palmitoylation alone (Suppl. Figure 2C). We show that while GFP alone diffuses inside but is not enriched in the ciliary compartment, a GFP fusion containing a short N-terminal region of PEF-1 (14 residues containing the MGCxxS/T myristoylation and palmitoylation motif), which we name myr-palm-GFP, is sufficient to confer a PEF-1-like localization to the ciliary axoneme (including exclusion from the transition zone; see representative images and graphs in Fig. 1D). In contrast, the same GFP fusion construct with a C3S mutation (myr-GFP) creates a myristoylated form of GFP that is not ciliary enriched (Fig. 1D).

Enrichment of PEF-1 within the axoneme but excluded from the transition zone requires a functionally intact transition zone

We observed that both PEF-1::GFP and myr-palm-GFP are cilium-localized but largely excluded from the transition zone (TZ; Figs. 1C,D Suppl. Figure 2C). This ciliary zone of exclusion or 'CIZE' parallels what is seen

◀**Fig. 2**. PEF-1 is required for cilium-dependent dye-filling of sensory neurons and regulation of cilium shape. (**A**). Dye-filling assay schematic shows the fluorescent dye DiI (red) penetrating sensory neurons via structurally intact, environmentally-exposed head and tail ciliated endings. Defects in ciliary structures can result in an abnormal dye filling (Dyf) phenotype. (**B**). Assessment of amphid neuron dye-filling by fluorescence microscopy, and categorization as no dye-filling (Dyf), partial Dyf or normal (non-Dyf). The *pef-1* mutant has a strong dye-filling defect comparable to the *che-3* Dyf mutant, a positive control with short bulbous cilia. Each dataset represents the mean from 3 independent experiments (at least 15 animals were measured for each). Scale bar, 20 µm. (**C**). Phasmid neuron dye-filling defect of *pef-1* mutant analyzed as in (B). Scale bar, 20 µm. (**D**). Representative images of wt or *pef-1* mutant animals expressing a GFP reporter specifically in AWB neurons by way of the *str-1* promoter (*str-1p*::GFP). The surface area (μm^2) of the AWB cilia 'wings' at the ends of short or long 'branches' is significantly large in *pef-1* animals compared to wt. Scale bar, 2 µm. (**E**). The branch length (µm) of the long AWB cilium in *pef-1* mutant animals is significantly shorter compared to wt animals. (**F**). Representative images of wt or *pef-1* worms expressing a GFP marker specifically in AWC neurons (*ceh-36p*::GFP). The total surface area (μm^2) of the AWC cilium 'wings' is significantly larger in *pef-1* mutant animals compared to wt. Scale bar, 2 µm. (**G**). The length (µm) of AWC short and long cilium branches are significantly shorter in *pef-1* mutant animals compared to wt. (**H**). Representative images of a *gcy-5p*::GFP reporter expressed in the ASE neuron reveals a statistically-shorter cilium length for the *pef-1* mutant compared to wt. Scale bar, 2 µm. (**I**). The overall shape of the AFD dendritic ending, which can be observed with the *srtx-1p*::GFP AFD neuron-specific reporter, harbors numerous microvilli and one cilium (only overall shape and some microvilli are resolved). In the *pef-1* mutant, the shape of the AFD finger/cilium compartment shows a statistically-significant alteration in width-to-length aspect ratio (representative images on the left). Scale bar, 2 µm. Dots represent individual measurements. Tukey's honestly significant difference was used for significance (p-value). *, $p < 0.05$; **, $p < 0.01$; ***, $p < 0.001$; n.s., not significant.

with transmembrane ciliary proteins[57,58]. We hypothesized that the TZ, acting as a 'ciliary gate' that excludes the lipidated proteins (*i.e.*, limits their diffusion across/within the region), may be necessary for their strong enrichment distal to the gate and within the ciliary compartment. To test this, we introduced our PEF-1::GFP reporter into mutants that affect three known TZ functional modules implicated in ciliopathies[13,25,58,59]: (1) a scaffolding module consisting of MKS-5 and CEP-290; (2) an MKS module consisting of at least 12 proteins, many of which are membrane-associated; and (3) an NPHP module known to harbors two proteins, NPHP-1 and NPHP-4.

We find that disrupting the scaffolding proteins MKS-5 or CEP-290 causes PEF-1::GFP mislocalization, diminishing its enrichment within the ciliary region distal to the TZ and increasing its localization to the TZ (Fig. 1E). Mutation of the MKS module protein MKS-2, known to affect the localization of other proteins within the same module[57,58,60,61], does not as significantly alter the localization of PEF-1::GFP (Fig. 1E). Similarly, disruption of NPHP-4 (the 'core' NPHP module protein[62]) has no clear effect on PEF-1::GFP localization (Fig. 1E).

To query if the compartmentalization of PEF-1 by the transition zone may be a general property of myristoylated/palmitoylated proteins, we compared our localization results with the G protein -subunit GPA-13, which has the same lipidation motif (its N-terminus, MGCNFSS, matches the MGCxxS/T consensus). Indeed, GPA-13 is strongly enriched in the axoneme of cilia but distal to the TZ in a wild-type strain, whereas the protein disperses across the TZ (and is more abundant in the PCMC) in the *mks-5* and *cep-290* mutants (as well as the *mks-2* mutant); in contrast, localization is not significantly affected in the *nphp-4* mutant (Suppl. Figure 3). These findings show that the strong enrichment of two different myristoylated and palmitoylated proteins to the ciliary compartment (distal to the TZ) depend on a functionally intact TZ, and suggest that the NPHP module may not play an important role with regards to the 'gating' of lipidated proteins.

PEF-1 is required for normal cilium-dependent dye uptake in ciliated sensory neurons

As no mutant was available to study the function of PEF-1, we generated a full-deletion (null) allele of the *pef-1* gene using CRISPR/Cas9 engineering. The overall morphology (including body length) and developmental profile of *pef-1* mutant animals appears normal (Suppl. Figure 4A and 4B). In addition, the movement of the *pef-1* mutant animals appears normal (described later).

To test for a potential role for PEF-1 in cilium formation, we first carried out a dye-uptake assay. In wild-type animals, several head cilia, as well as tail cilia, are environmentally-exposed and their membranes can incorporate an externally-supplied lipophilic dye (DiI); the dye then disperses throughout the respective sensory neuron cell bodies[63] (Fig. 2A). A dye-filling defect often occurs when ciliary axonemes are absent or shortened, as for example seen upon disrupting intraflagellar transport (IFT), which is required for cilium formation and maintenance[64–66].

The *pef-1* null mutant shows a prominent dye-filling defect in amphid (head) ciliated neurons, comparable to that of the IFT-dynein mutant *che-3* used as a positive control (Fig. 2B). A dye-filling defect is also observed in phasmid (tail) ciliated neurons (Fig. 2C). In addition, dye-fill defects were also observed in two additional CRISPR/Cas9-generated *pef-1* missense alleles of *pef-1* that target its myristoylation and palmitoylation lipid modification sites (described later). Importantly, the dye-filling phenotypes of the *pef-1* null mutant can be partially rescued by expression of a wild-type *pef-1* transgene (Suppl. Figure 4C). We note that this 'global' dye-filling defect in the *pef-1* mutant might involve non-cell autonomous effects, or perhaps more likely, additional sensory neurons wherein *pef-1* expression is low and may not be observed in the transcriptome studies (but in the case of phasmids is detectable with PEF-1 endogenously tagged with GFP; Suppl. Figure 2B). Together, these

results show that in *C. elegans*, PEF-1 is required for correct dye-filling of ciliated sensory neurons, and thus may help establish and/or maintain at least some, if not all, ciliary structures.

PEF-1 influences the structures of diverse classes of cilia

To directly visualize if disrupting PEF-1 results in cilium structure anomalies, we used a panel of soluble GFP reporters, expressed in different ciliated sensory neurons, that reveal the overall shapes/structures of cilia. Strains harboring reporters expressed in the following neurons were made: AFD, AWC and ASE neurons, wherein endogenous *pef-1* expression is strong (Fig. 1B); AWB neuron, which exhibits lower expression; and as a control the ASI neuron, which has no detectable *pef-1* expression. Confocal microscopy was performed to measure the overall lengths and/or shapes of the respective ciliary structures (see Fig. 1A schematics).

"The AWC and AWB neurons both have two branched or 'wing-like' membranous dendritic endings, although notably, only one branch in the former structure contains a cilium, whereas both branches harbor cilia in the latter structure. In the *pef-1* mutant, the single-ciliated AWC and double-ciliated AWB wing-like endings are present but show statistically-significant increases in membrane area compared to wild-type; furthermore, shortened branches are present (Fig. 2D–G). Our AWC membrane area for wild-type is notably smaller than that previously reported (~7 μm^2 vs. 11.6 μm^2[67]), potentially due to several factors, including the level of expression of the AWC cilium GFP reporter, imaging, and tracing of the wings for measurements (in our case, automatic segmentation based on fluorescence intensity; see Materials and Methods).

The length of the rod-shaped ASE cilium is shorter in the *pef-1* mutant (5.65 ± 0.5 µm) compared to wild-type (6.8 ± 0.7 µm) (Fig. 2H). In comparison, ASI cilium length is not affected in the *pef-1* mutant (Suppl. Figure 4D). Lastly, a statistically-significant proportion of AFD neuron endings—which consist of a bulbous compartment from which emanate numerous microvilli ('fingers') as well as a single cilium[68,69]—exhibit a more extended morphology in the *pef-1* mutant compared to wild-type (Fig. 2I; aspect ratio is measured). These findings reveal that PEF-1 is not required for the formation of cilia (ciliogenesis) per se, but does have an influence on the development and/or maintenance of the structures of several classes of cilia, consistent with the observed dye-filling defects.

To complement our fluorescent reporter analyses, we directly visualized the ciliary ultrastructures of the *pef-1* null mutant using transmission electron microscopy (TEM) (Fig. 3). In the proximal-most region of the channel (rod-shaped) ciliary axonemes, the transition zone (TZ) regions appear normal (Fig. 3A), exhibiting the characteristic Y-shaped connections between the axoneme and overlying membrane[26,27,70]. Distal to this, in the ciliary proximal (middle) segments, the expected doublet microtubules[70] are visible, although many look incomplete and have 'open' B tubules that do not connect to the A tubules to form intact doublets (Fig. 3A). Ultrastructural defects are increasingly apparent in the more distal region of the channel cilia. While this ciliary subdomain (distal segment) is indeed present and bounded by a membrane, the singlet microtubules which are readily identified in wild-type cilia[70] are absent or indistinct in the *pef-1* mutant (Fig. 3A). Instead, electron-dense amorphous material interspersed with occasional singlet-like, microtubule-like structures fill the region. While AWC wings extend properly and AFD fingers and cilia appear largely normal in the *pef-1* mutant (Fig. 3H–M), in one of the three animals we sectioned, the ciliary ending and actin-rich fingers of one of the AFD neurons was displaced posteriorly by ~2 µm, consistent with the elongated morphology observed using the fluorescent marker (Fig. 2I). Finally, in AWA and AWB (but not AWC) cilia, fewer microtubules are seen compared to wild-type animals (Fig. 3B–G).

The ultrastructural anomalies of the channel cilia are potentially indicative of either a defect in microtubule formation (biogenesis)—or potentially, given the presence of amorphous material and potential single microtubule remnants (Fig. 3A)—of a microtubule degeneration phenotype. This could be similar to that observed in the *che-10* mutant, where cilia are made but degenerate during post-embryonic development[69,71]. We took advantage of the dye-filling assay as a proxy to test whether the ciliary integrity of the *pef-1* mutant might worsen during development. We find that as previously described[72], the earliest larval stages (day 1 *ex utero*) of wild-type animals have incomplete/reduced dye-filling compared to later stages (days 2–4), which have close to 100% dye-filling (Suppl. Figure 5). While the *pef-1* animals dye-fill to an extent comparable to wild-type at the earliest stage, their ability to dye-fill at later stages becomes worse (Suppl. Figure 5). This is consistent with the potential degeneration of cilia—in particular the distal region, which is important for correct dye-filling—during development. An alternative but not mutually exclusive possibility is that cilium formation in the *pef-1* mutant may be impaired during development relative to wild-type animals.

Altogether, our observations reveal that loss of PEF-1 results in ultrastructural changes to diverse cilia, and hint at—particularly within the distal regions of rod-shaped cilia—potential degeneration of ciliary microtubule structures.

PEF-1 plays a role in cilium-dependent chemosensory, thermosensory and photosensory behaviors

Having established a function for PEF-1 in sculpting and potentially maintaining the structures of different cilia, we sought to determine if the phosphatase also regulates cilium-dependent sensory processes and behaviors. To this end, we conducted behavioral assays that test the functions of different classes of cilia, namely chemosensation (attraction and avoidance), thermosensation and photosensation[34,35,37,43,73].

Attraction to and repulsion from soluble compounds

The strong expression of *pef-1* in the ASE and AWC neurons suggested a potential role for the phosphatase in the detection—and chemotaxis towards—a soluble or volatile compound, namely salt (NaCl) or alcohol (isoamyl alcohol), respectively. We carried out standard chemotaxis assays and found that *pef-1* mutants have a lower attraction to salt compared to wild-type animals (Fig. 4A). The phenotype is not as severe as that of the *che-*

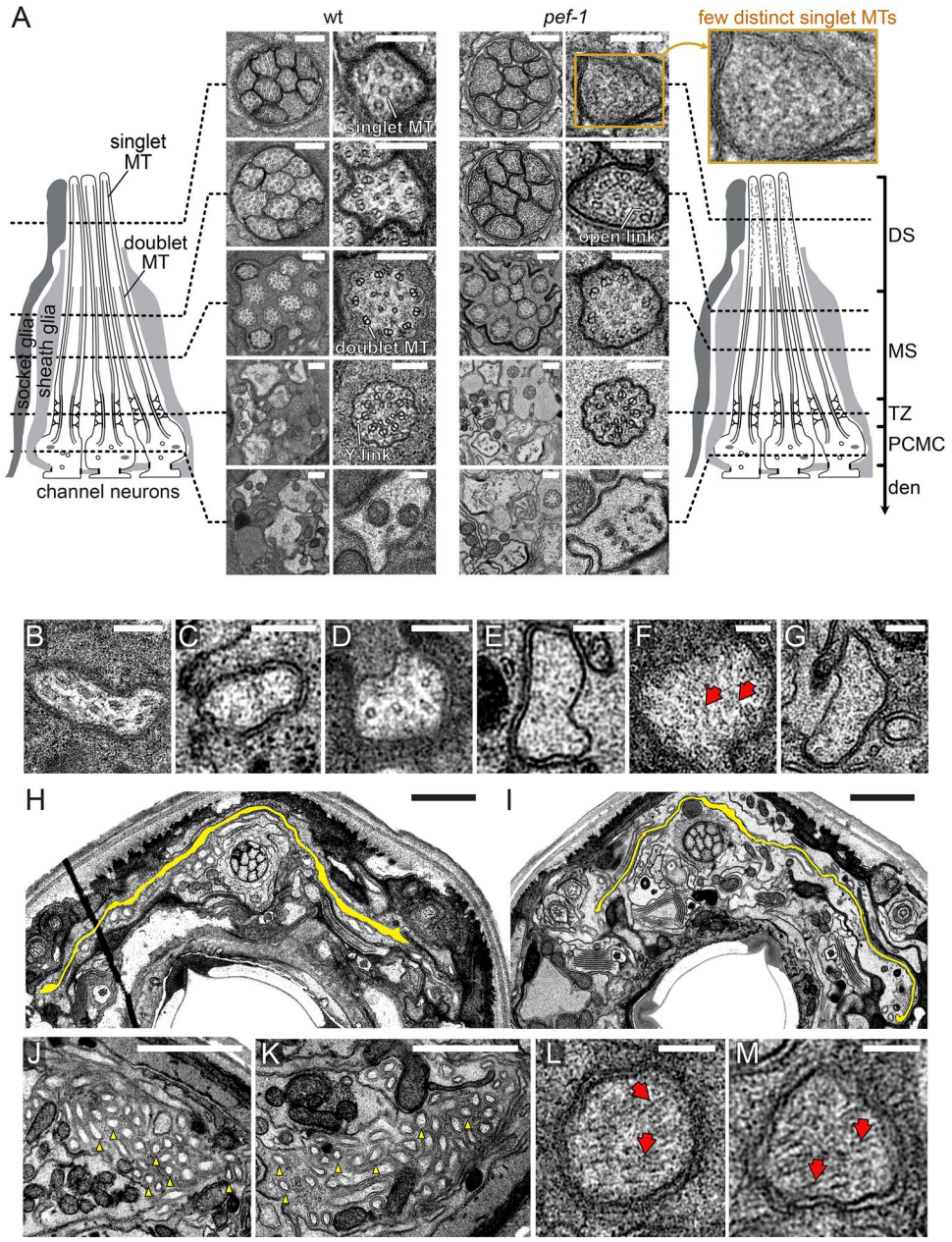

Fig. 3. Loss of PEF-1 leads to ciliary ultrastructure defects. (**A**). Analysis of wt and *pef-1* mutant amphid channel neurons by transmission electron microscopy. Representative cross-section images for the periciliary membrane compartment (PCMC), transition zone (TZ), middle segment (MS) containing doublet microtubules (MTs), and distal segment (DS) containing singlet MTs are shown (den, dendrite). For each genotype, the right image of an image pair is a magnified view of one ciliated neuron from the left image. *pef-1* mutant distal MTs are difficult to resolve (top row), and some doublet MTs in the MS appear incomplete, exhibiting open links. *pef-1* mutants resemble wt animals closer to the ciliary base. Scale bars: left, 200 nm; right, 100 nm. (**B-G**). Representative images of wt and *pef-1* mutant AWA, AWB, and AWC neuron cilia (B,D,F and C,E,G, respectively). Note that AWA and AWB neurons have fewer microtubules in the *pef-1* mutant. Scale bars: 100 nm. Red arrows, horizontal microtubules. (**H,I**). The AWC neuron cilium wing, highlighted in yellow, in wt (H) and *pef-1* mutant (I). Scale bar: 500 nm. (**J,K**). AFD neuron fingers (yellow arrowheads) in wt (J) and *pef-1* mutant (K). Scale bar: 500 nm. (**L,M**). AFD cilium in wt (L) and *pef-1* mutant (M). Scale vars: 100 nm. Red arrows, horizontal microtubules.

3 mutant, which has a defect in retrograde IFT and exhibits severely compromised ciliary structures with a bulbous accumulation of IFT proteins at their tips[69,74]. In contrast, the attraction of the *pef-1* mutant to isoamyl alcohol does not appear to be affected (Fig. 4B).

C. elegans avoids high-osmolarity environments such as glycerol and sucrose[35,38]. This defensive behavior depends on functionally-intact cilia (ASH neurons), such that IFT- and BBS-defective mutants exhibit

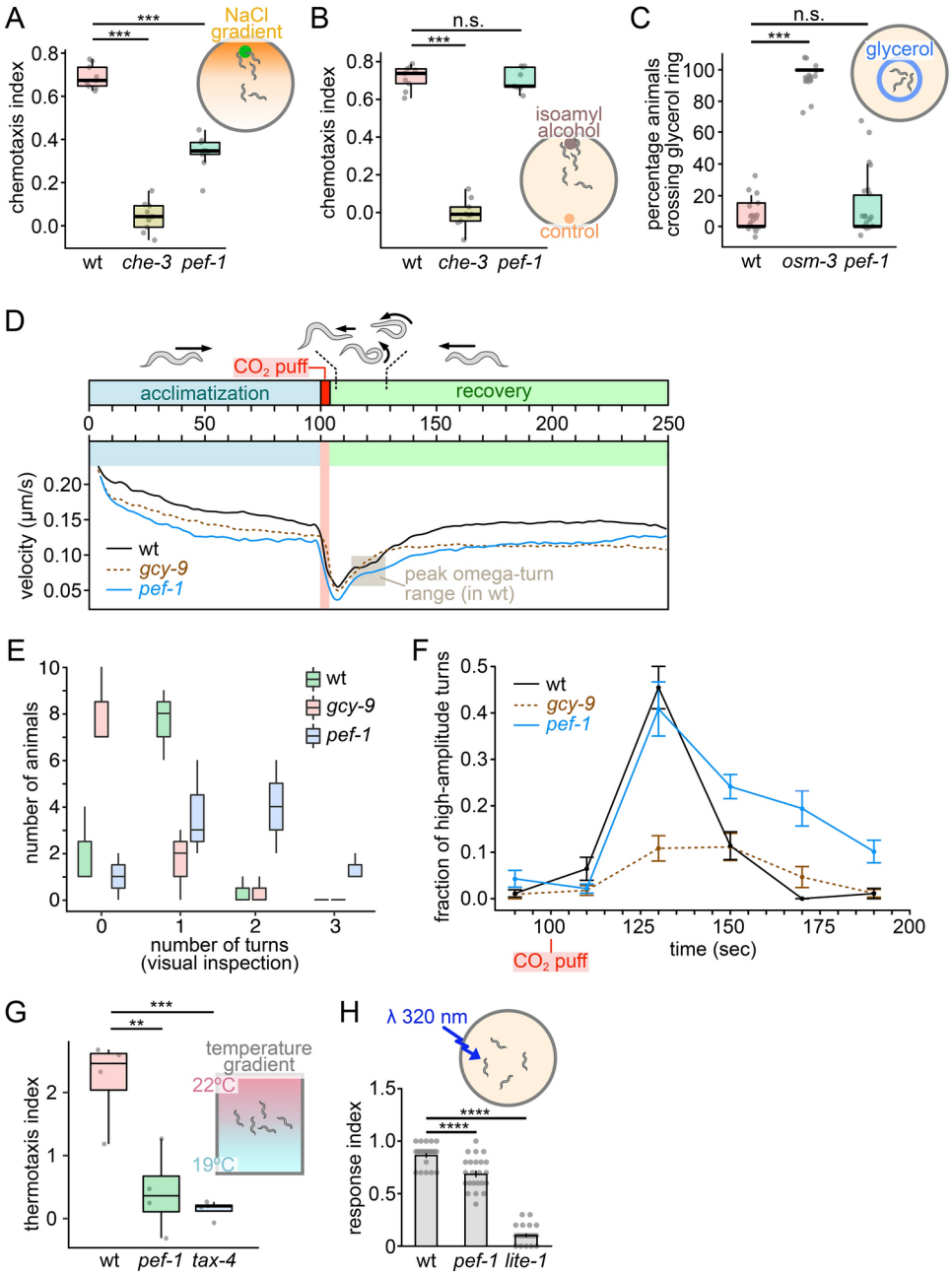

osmoavoidance (*osm*) phenotypes[35,53,69]. The *pef-1* gene does not appear to be (abundantly) expressed in ASH neurons, and unlike the IFT gene mutant *osm-3*[75], the *pef-1* null mutant behaves like wild-type (*i.e.*, shows an avoidance phenotype) when confronted with a high-osmolarity glycerol barrier (Fig. 4C).

Avoidance response to CO_2 stimulus

The *pef-1* gene shows strong expression in the BAG neuron (Fig. 1A,B), which plays an essential role in mediating an acute, aversive response to an elevated CO_2 level that is harmful to *C. elegans*[76]. Other neurons that express *pef-1*, including the O_2-sensing neurons URX, AQR and PQR, as well as ASE and AFD (Fig. 1B), also participate in this avoidance response[76–79].

To determine if PEF-1 regulates the response of *C. elegans* to CO_2, we monitored the behavior of animals subjected to an elevated level of the gas using a Multi-Worm Tracker (MWT). The MWT records several kinetic parameters of individual animals, including velocity, angular velocity and direction bias[80]. Each MWT-CO_2 assay tracks 150–200 animals during three stages totalling 250 s (Fig. 4D): a 100-s acclimatization period (shown in blue); a 4-s pulse of 10% CO_2 (red); and finally, a 146-s recovery period (green).

Wild-type animals exhibit a stereotypical behavior during the assay (Fig. 4D and Movie 1). First, they reduce their velocities during acclimatization. Following the CO_2 pulse, animals slow down abruptly, stop and reverse direction briefly. Animals then typically execute one high-amplitude ('omega') turn (Fig. 4E), where the head and tail join to form a compact (omega-shaped) loop (Fig. 4D). Both the *pef-1* mutant and a *gcy-9* mutant (control) respond to the CO_2 stimulus by slowing down (Fig. 4D; Movies 2 and 3). However, the fraction of animals that

◀**Fig. 4**. PEF-1 function is required for cilium-dependent chemosensory, thermosensory and photosensory behaviors. (**A, B**). Chemotaxis responses of wt, *che-3* and *pef-1* mutant animals to a gradient of NaCl (**A**) or 1:100 dilution of isoamyl alcohol (**B**). The chemotaxis index is significantly different for salt but not isoamyl alcohol. The *che-3* mutant control has a defect in retrograde IFT and exhibits severely impaired cilia**.** (**C**). Osmolarity avoidance of wt, *osm-3* and *pef-1* mutant animals when placed in an 8 M glycerol ring. Most of the wt or *pef-1* animals avoid crossing the barrier whereas the *osm-3* mutant (lacking ciliary distal segments) is defective in osmosensation and crosses the barrier. Dots represent individual plates. Tukey's honestly significant difference was used for significance (p-value). n.s., $p > 0.05$; ***, $p < 0.001$. (**D**). *C. elegans* responses to a noxious puff of CO_2 as measured in a Multi-Worm Tracker (MWT) experiment. Synchronized animals are plated with no food and left to acclimatize to the environment for 100 s. A 10% CO_2 gas stimulus is then delivered to the animals and their responses recorded until 250 s. In wt animals, a stereotypical behavior includes: velocity (μm/s) decreases during acclimatization; a sharp reduction in speed and stopping after the CO_2 puff; typically one high-amplitude (omega) turn occurs; finally, animals recover and increase their speeds. The *gcy-9* mutant slows down following the CO_2 pulse but generally does not execute an omega turn. Similar to wild-type animals, *pef-1* mutant animals slow down during acclimatization then stop after the CO_2 puff. However, they have a prolonged response (see panels E and F) and do not recover their speed rapidly. (**E**). Visual inspection of the number of omega turns executed by animals following the 10% CO_2 puff. *gcy-9* mutant animals often fail to make an omega turn, whereas most wt animals perform one turn. A higher proportion of *pef-1* mutant animals undertake 1, 2 or 3 turns. (**F**). Graph showing the fraction of animals executing high-amplitude turns during different stages of the MWT-CO_2 assay (automated quantitation of turns). *gcy-9* mutants exhibit a greatly attenuated response, with few turns compared to wt and the *pef-1* mutant following the CO_2 puff at 100 s. Compared to wt animals, which rapidly return to a low fraction of high-amplitude turns after the peak response (~ 130 s), *pef-1* mutant animals exhibit a prolonged duration of time executing high-amplitude turns. (**G**). *pef-1* animals exhibit impaired thermotaxis in a linear temperature gradient (19-22°C). Wild-type animals are attracted to the warmer temperature (positive thermotaxis index) and migrate towards the edge of the plate. In contrast, *pef-1* mutants behave similar to *tax-4* animals, exhibiting a low thermotaxis index and reduced preference for their cultivation temperature. Each dot represents the thermotaxis index of a biologically independent assay comprised of at least 300 animals. Tukey's honestly significant difference was used for significance (p-value). **, $p < 0.01$; ***, $p < 0.001$. (**H**). *pef-1* mutant animals exhibit a defect in photosensory avoidance behavior. Head avoidance responses to UV-A light (2 s, 350 ± 25 nm, 406 mW/mm^2) were scored as described in the Materials and Methods. The response rate in *pef-1* was reduced compared to wt but not as strongly as for *lite-1*. ($n \geq 10$). One-way Anova with Bonferroni's test was used to test for significance. ****, $p < 0.0001$.

performs high-amplitude turn(s) is significantly lower for the *gcy-9* control mutant (Fig. 4E,F Movie 2); this is expected given the role of the guanylyl cyclase in this response[81,82]. In contrast, *pef-1* mutants perform a greater number of turns on average and for a prolonged period of time after the stimulus (Fig. 4E,F; Movie 3). This suggests that PEF-1 modulates the response to the CO_2 stimulus. Notably, *pef-1* mutants lacking myristoylation/palmitoylation signals also exhibit an overactive response (see below), confirming the role of the PPEF-type phosphatase in this avoidance behavior.

Thermotaxis

Several ciliated sensory neurons, in particular AFD and to a lesser degree AWC, ASI and ASJ, form an exquisitely sensitive and precise thermosensory network that helps *C. elegans* move (thermotax) toward its preferred (cultivation) temperature[40,83]. Given the robust expression of *pef-1* in AFD and AWC neurons (Fig. 1B), we tested the ability of the *pef-1* mutant to navigate a thermal gradient ranging from 19℃ to 22℃. Our assays show that *pef-1* mutants are not able to thermotax like wild-type animals. Rather than favor movement towards their cultivation temperature (20℃), the *pef-1* mutant animals showed a significantly more random distribution between the higher and lower temperatures, yielding a thermotaxis index of less than 0.5, compared to over 2 for wild-type (Fig. 4G; see also materials and methods). Notably, the *pef-1* thermotaxis phenotype is similar to that of the *tax-4* mutant, which lacks the alpha subunit of a cGMP-gated channel necessary for sensory transduction in thermosensory neurons[84].

Photoavoidance

Nematodes like *C. elegans* lack a distinct light-sensing organ (eye) but have a robust negative phototaxis response to avoid UV light[85]. This response depends on a G protein signal transduction pathway initiated by a photosensitive protein (LITE-1) that is unrelated to rhodopsin, and which operates in several ciliated sensory neurons[49,86]. We tested *pef-1* mutant animals in a photo-avoidance assay and found a statistically-significant decreased response relative to wild-type; however, this attenuated response is not as pronounced as that of the *lite-1* mutant (Fig. 4H).

Altogether, our findings suggest that *C. elegans* PEF-1 plays roles in ciliated sensory neurons that control various sensory modalities and regulate behaviors, including chemosensation, thermosensation, and to a lesser degree, photosensation.

Myristoylation and palmitoylation is required for the ciliary functions of PEF-1

Many PPEF-type phosphatases found across protists and metazoans have evolutionarily conserved myristoylation and palmitoylation signals at their N-terminus (see references[42,55,87,88] and Suppl. Figure 1). To determine if the

lipid modifications of PEF-1 are necessary for the biological function of the phosphatase, we first confirmed the finding by Ramulu and Nathans[42] that PEF-1::GFP bearing G2A and C3S mutations—which alter its ability to be myristoylated and palmitoylated, or palmitoylated, respectively—indeed cause the mislocalization of the protein (no longer concentrated at the cilia; Suppl. Figure 2C). Next, we used CRISPR/Cas9 to engineer into the genomic *pef-1* locus two separate strains, one bearing the G2A, or the C3S mutation. These *pef-1* G2A and C3S mutant strains were then subjected to various assays wherein the *pef-1* null mutant previously showed a cilium structure phenotype (dye-filling to test for ciliary integrity; AWB and AWC wing area; ASE cilium length) or a cilium-dependent behavioral defect (chemotaxis towards NaCl and CO_2 avoidance). In all cases, the *pef-1*(G2A) and *pef-1*(C3S) mutants displayed phenotypes comparable (if not nearly identical) to that of the *pef-1* null allele; this includes the prolonged response to the CO_2 stimulus compared to wild-type (Figs. 5A,B). Altogether, these analyses of the PEF-1 G2A and C3S variants reveal the importance of myristoylation and palmitoylation for the ciliary functions of the protein phosphatase.

Discussion

Early two-dimensional gel electrophoresis analyses of isolated *Chlamydomonas* motile cilia revealed several hundred distinct protein species, providing evidence that the cilium is a complex cellular organelle[89]. Since then, numerous complementary studies, including proteomics, functional genomics, comparative genomics (bioinformatics), genetics, and transcriptome analyses have aimed to identify complete 'ciliomes' from multiple species[90–98]. All approaches have limitations, however, and may for example fail to uncover low-abundance proteins, membrane-associated proteins, poorly-expressed genes, and/or genes only expressed in specific metazoan cell types[99].

Here, we used single-cell transcriptome data from *C. elegans* to enrich for genes specifically expressed in cells (sensory neurons) bearing cilia (Suppl. Table 1), and identified the evolutionarily-conserved PPEF (Serine/threonine-protein phosphatase with EF-hands) family gene, *pef-1*, as a noteworthy target for further analysis. We confirmed that *pef-1* is expressed in ciliated sensory neurons and that its protein product specifically localizes distal to the transition zone in diverse types of cilia in the head and tail of the animal (Fig. 1C).

Our dye-filling experiments first suggested a potential defect in the (normal) exposure of ciliary structures to the external environment (Fig. 2A–C). Analyses involving cell-specific fluorescent reporters corroborated this finding, revealing that *C. elegans* lacking PEF-1 have defects in the structures of various classes of cilia (Fig. 2D–I). The rod-shaped ASE cilium is shorter; the 'wings' (elaborate membraneous structures) of the AWB and AWC cilia have a larger surface area and different branch lengths; and the morphology of the AFD ciliated ending is abnormal. Importantly, TEM analyses identified loss of ultrastructural integrity for some cilia, in the middle

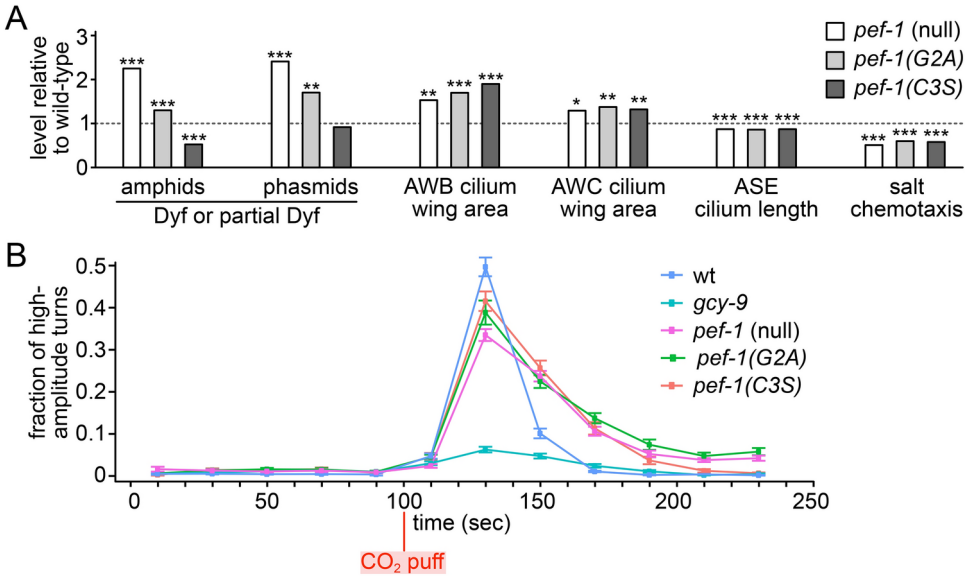

Fig. 5. The function of PEF-1 depends on myristoylation and palmitoylation. (**A, B**). Myristoylation and palmitoylation are both required for the functions of PEF-1. *pef-1(G2A)* and *pef-1(C3S)* mutant animals exhibit, to varying degrees, the same cilium-associated phenotypes as that of the *pef-1* (null) mutant. The bar graph (top) shows that all three *pef-1* mutant strains exhibit, relative to wt: decreased (absent or low) amphid and phasmid neuron dye-filling; increased AWB and AWC 'wing' cilia area; decreased ASE cilium length; and reduced ability to chemotax towards salt (NaCl). All assays were carried out in parallel to those shown in Fig. 2B-H and Fig. 4A, and levels shown are relative to wild-type, which has been normalised to 1.0. The plot (bottom) shows the proportion of animals executing high-amplitude turns after a CO_2 stimulus delivered at 100 s (assays carried out as in Fig. 4E,F). The prolonged response of the *pef-1(G2A)* and *pef-1(C3S)* mutants following the stimulus is similar to that of the *pef-1(null)* mutant. Tukey's honestly significant difference was used to test for significance. *, $p < 0.05$; **, $p < 0.01$; ***, $p < 0.001$; n.s., not significant.

segment and particularly towards the distal end (distal segment), in the form of indistinct and thus potentially degenerated microtubules (Fig. 3). Together, these findings show that unlike intraflagellar transport (IFT) proteins[22,24,100,101], PEF-1 is not essential for cilium formation (ciliogenesis) per se. Instead, the phosphatase appears to regulate morphological characteristics of some but not all cilia, including their length and membrane elaborations. In addition, or alternatively, PEF-1 may be required for the maintenance of these microtubule-based ciliary structures; this may stem from the influence of the phosphatase on the function of the intraflagellar transport (IFT) system, kinases, depolymerizing kinesins, or tubulin post-translational modifications—all of which are known to participate in cilium length control, shape, and/or maintenance[2,8,13,15,19,23,28]. Potentially consistent with this possibility, we find that the dye-filling phenotype in the *pef-1* mutant becomes worse over a 4-day period of development, from L1 larvae to young adults (Suppl. Figure 5).

Disruption of PEF-1 causes reduced chemotaxis towards an attractant, NaCl (Fig. 4A). Since the mutant animals move normally, this phenotype likely results from a salt-sensing or signaling defect in the ASE neuron[102,103]. The reduced exposure of amphid (head) cilia to the environment, which is suggested by the dye-filling defect observed in the *pef-1* mutant (Figs. 2A–C), could in principle fully or partially account for this phenotype[65,69,104]. However, we also observed defects in thermotaxis (Fig. 4G), which depends on AFD (as well as AWC) neurons that are not directly exposed to the environment[40,69,105]. This suggests that the altered ciliary structures and functions in these neurons could directly underlie the behavioral defects. Interestingly, PEF-1 may not act in all classes of cilia and/or may have functions that are not revealed in certain behavioral assays. The *pef-1* mutant displays normal chemotaxis towards isoamyl alcohol and can avoid a high-osmolarity barrier (Figs. 4B,C). Also notable is that the major reported role for *Drosophila* RDGC is in (non-ciliary) rhabdomeric photoreceptors[46], and the photoavoidance response in the *C. elegans pef-1* mutant is also partially impaired (Fig. 4H). This latter finding further confirms a ciliary role for the phosphatase, as photosensation in the nematode depends on ciliated neurons, including ASJ, ASK and ASH[85,86].

Given the strong expression of *pef-1* in the BAG ciliated neuron, we also tested if disruption of the phosphatase influences the animal's aversive reaction to CO_2, which at an elevated concentration is toxic to *C. elegans*[76,106,107]. We find that *pef-1* mutant animals can sense the gas, first slowing their movement after exposure to the CO_2 puff (Fig. 4D). However, compared to wild-type, they execute a greater number of omega-turns, for a longer period of time, in an attempt to reorient away from the noxious stimulus (Fig. 4E,F). This suggests that PEF-1 might help downregulate the signaling pathway required for amplification if this response, which involves the cGMP-producing guanylyl cyclase GCY-9 (Fig. 4D–F) and TAX2/TAX4 cGMP-dependent calcium channel[76,81,82].

The PPEF family of phosphatases are widely conserved across ciliated eukaryotes but absent from fungi and plants[41] which secondarily lost cilia during evolution[21,90]. This may indicate that prior to the emergence of metazoans, the primordial cellular function for PPEF phosphatases was associated with cilia. Our findings support such a possibility, since *C. elegans* PEF-1 contributes to the formation and potentially maintenance of different types of cilia, and its function is needed for the correct execution of cilium-dependent behaviors.

PPEF phosphatases from other metazoans may also have ciliary functions, and there is evidence that at least one has acquired an alternate, non-ciliary function. By far the best characterized member of the PPEF family is RDGC in *Drosophila*, whose disruption was shown by the O'Tousa laboratory in 1992 to cause the light-induced degeneration of photoreceptors[45,46]. Notably, fruit fly photoreceptors are not ciliary (microtubule-based) like in vertebrates, but instead, comprise rhabdomeres with numerous actin-based microvilli[108–111] (Fig. 6A). In these membrane-ensheathed compartments, RDGC is thought to dephosphorylate the G protein-coupled receptor (GPCR) rhodopsin as part of a light-dependent signaling cascade involving the heterotrimeric G_q protein, arrestin, phospholipase C (PLC), and Protein Kinase C (PKC)[46,47,109,112,113]. RDGC is also implicated in the dephosphorylation of another player in the phototransduction pathway, namely a TRP-family Ca^{2+} channel[114]. Notably, both GPCRs and TRP channels function in comparable pathways in ciliary compartments[115–117]. The roles of RDGC in a non-ciliary compartment, both in *Drosophila* and potentially other metazoans, is summarized in Fig. 6A.

Aside from their conserved phosphatase domain, RDGC and other PPEF proteins, including *C. elegans* PEF-1, contain two flanking regions relevant to the calcium-dependent regulation of signal transduction pathways. One is an N-terminal IQ domain, which in *Drosophila* RDGC and the two human PPEF proteins (PPEF1 and PPEF2) have been experimentally confirmed to interact with calmodulin (CaM)[113,118]. CaM contains four Ca^{2+}-binding EF-hands and has established roles in vision, olfaction, and other processes, including muscle contraction[119]. The second is a C-terminal domain containing EF-hands, which in *C. elegans* PEF-1 has confirmed Ca^{2+}-binding properties[120].

In addition, consensus sites for myristoylation and palmitoylation (N-terminal MGCxxS/T motif) are present in *C. elegans* PEF-1[42], *Drosophila* RDGC[88], Kinetoplastid (*Leishmania*) PPEF[87], as well as mammalian PPEF1 (Suppl. Figure 1A; lipid modifications are experimentally confirmed in the first three). In this study, we found that both modifications are required for PEF-1 enrichment within the axonemal region of cilia (Fig. 5A), consistent with the previous findings of Ramulu and Nathans [42]. Mechanistically, we ascribe this ciliary targeting and enrichment to the modifications, since GFP itself becomes enriched in cilia when it harbors the MGCxxS/T motif, and like PEF-1 is no longer specifically enriched in cilia when it loses both modifications or palmitoylation alone (Fig. 1D). We also show that ciliary enrichment for not only PEF-1 but also the myristoylated/palmitoylated GPA-13 protein depends on the transition zone (TZ) (Fig. 1E and Suppl. Figure 3), which excludes membrane-associated proteins and acts as a 'ciliary gate' or membrane diffusion barrier, ostensibly because it forms a lipid microdomain[26]. Particularly important in this regard are the core scaffolding proteins MKS-5 (ortholog of mammalian RPGRIP1L) and CEP-290 (CEP290), and to a lesser degree the so-called core 'MKS module' protein MKS-2 (MKS2/TMEM216), all of which are implicated in ciliopathies[13]. Both lipid modifications—which together likely strengthen membrane attachment[54]—are required for the various cilium-associated functions

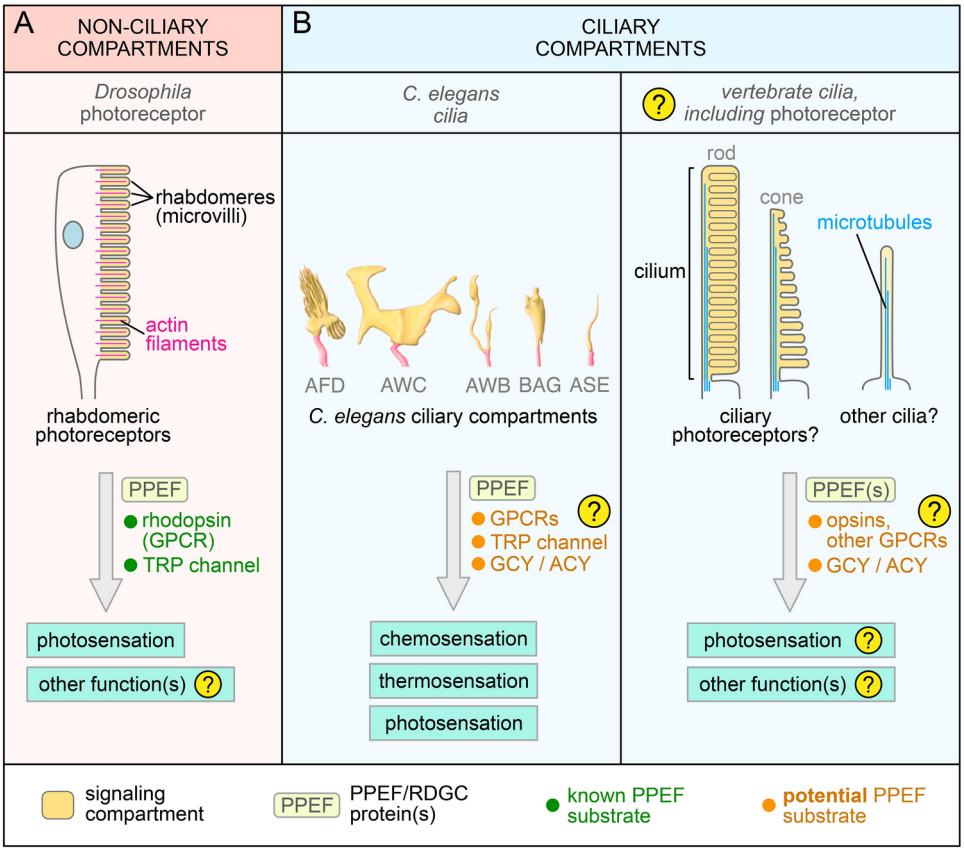

Fig. 6. Model: PPEF family phosphatase proteins function in non-ciliary and ciliary sensory compartments. (**A**). The canonical PPEF-family phosphase from *Drosophila*, retinal degeneration C (RDGC), is known to regulate signaling in rhabdomeric (non-ciliary) photoreceptors by influencing two substrates (shown in green), namely the light-sensing GPCR rhodopsin and a calcium TRP channel (see text for details). In both *Drosophila* and other metazoans, PPEF proteins could potentially play signaling roles in other non-ciliated cell types (indicated as a question mark). (**B**). The *C. elegans* PPEF protein, localizes to several types of cilia and is required for several cilium-dependent functions, namely chemosensation, thermosensation and photosensation. Its substrates are unknown (shown in orange) but could also include GPCRs, TRP channels, and potentially components of cyclic nucleotide signaling, including guanylate cyclases (GCY) and adenylate cyclase (ACY) that regulate the sensory behaviors. In other metazoans, including vertebrates, PPEF proteins may play currently-unknown roles in ciliary photoreceptors (rods/cones) or other types of cilia, potentially affecting opsins, GPCRs and other signaling proteins.

of PEF-1, including dye-filling via intact cilia, cilium structure properties, and chemosensation (salt chemotaxis and CO_2 avoidance) (Fig. 5A,B).

Collectively, the studies conducted on *Drosophila* RDGC and our work on *C. elegans* PEF-1 suggest that PPEF phosphatases can regulate membrane-associated sensory/signaling processes, in either a non-ciliary, or a ciliary, context. In the case of rhabdomeric and ciliary photoreceptors, many of the signaling components that function together with the PPEF phosphatases are evolutionarily related, including GPCRs, GPCR kinase, arrestin (modulates GPCRs), G proteins, PLC and TRP channels[109,110,121]. Based on these findings, we present a model, wherein PPEF phosphatases influence signaling pathways in non-ciliary (Fig. 6A) or ciliary (Fig. 6B) compartment(s). The clearest evidence for non-ciliary functions is thus far restricted to *Drosophila* rhabdomeric photoreceptors, while evidence for ciliary functions is restricted to our work.

Although mammalian *PPEF2* is known to be expressed in the retina, and its encoded protein has been detected in the mouse ciliary phosphoreceptor proteome[92], a mouse *PPEF1-PPEF2* double knockout mouse perhaps surprisingly does not show detectable differences in rhodopsin phosphorylation levels, or retinal degeneration[51]. It is possible in mammals at least, the major effector of opsin dephosphorylation is not PPEF1 or PPEF2, but the related PPP phosphatase, Protein Phosphatase 2A (PP2A), which has recognized roles at centrioles/centrosomes and cilia[122–124]. This may reflect promiscuity and/or evolving substrate specificity amongst different PPP phosphatases.

Mammalian PPEF1 and PPEF2 proteins are poorly characterized, and currently have no known ciliary functions. However, mutational analysis of a family presenting with nonsyndromic high myopia was found to have a variation in an evolutionarily conserved residue of PPEF2[125]. Interestingly, in a zebrafish screen for genes with retinal functions, PPEF2 was selected for morpholino-knockdown phenotypic analysis, and shown to result

in a small eye-phenotype potentially indicative of ciliary photoreceptor degeneration[126]. This, combined with our discovery that *C. elegans* PEF-1 functions in a variety of ciliated sensory neurons and is cilium-localized, provides impetus for proposing in our model (Fig. 6B) that the mammalian PPEF counterparts could potentially play regulatory roles in certain ciliated cell types, and as such, are worth exploring as novel ciliopathy candidates.

Materials and methods

C. elegans strains and maintenance

All *C. elegans* strains used in this study are listed in Supplementary Table 2. Strains were grown and cultured according to standard procedures on nematode growth medium (NGM) plates with OP50 bacteria as a food source and maintained at 20C. GFP-tagged protein constructs were introduced into listed genetic backgrounds by standard *C. elegans* mating methods. Genotyping of the strains generated was performed by single-worm PCR. The wild-type *C. elegans* used was the strain Bristol. The following strains were kindly provided to us: Dr. Sengupta: *N2[str-3p::srg-36::gfp]* and *oyIs50[ceh-36p::gfp]*, Dr. Moerman *pef-1(gk5346[loxP + Pmyo-2::GFP::unc-54 3' UTR + Prps-27::neoR::unc-54 3' UTR + loxP])* created using CRISPR-Cas9 genome engineering. Several *C. elegans* strains were obtained from the *Caenorhabditis* Genetics Center (CGC), namely *lin-15B&lin-15A(n765);kyIs104[str-1p::gfp], osm-3(p802)* and *che-3(e1124).*

Generation of GFP translational fusion protein constructs

P*bbs8*::PEF-1::GFP constructs and their variants (G2A and C3S) were was generated by creating a translational fusion construct using Gibson Assembly. Transgenic worms expressing the above construct were generated by gonadal transformation of N2 hermaphrodites via microinjection and subsequent screening for transgenic progeny. A GFP fusion construct containing at its N terminus the first 14 amino acids of PEF-1 (MGCGPSSGRQNPST, which contains the myristoylation/palmitoylation consensus sequence MGCxxS/T) was generated together with a palmitoylation-deficient construct (C3S mutant). Strains bearing all constructs were generated and analyzed by confocal microscopy.

Myristoylation- and/or palmitoylation-defective pef-1 mutant strains

Strains harboring point mutations at the lipid modification sites (residues G2 and C3) of *pef-1*, namely PHX2678 (*pef-1*(syb2678-G2A)) and PHX2989 (*pef-1*(syb29890-C3S)), were generated by CRISPR-Cas9 genome engineering by SunyBiotech (https://www.sunybiotech.com) and verified by sequencing.

Methods for identifying potential cilia genes

Identification of genes with a potentially core role in ciliated neurons was carried out using the dataset from Cao and colleagues[44]. This single cell RNA-seq dataset contains transcriptomic data from the L2 stage of *C. elegans* at which point the cilia have formed. Cells that were identified by subtype and consensus expression values for major cell types in *C. elegans* were calculated. We used both the ciliated neuron-enriched genes and oxygen sensory-enriched genes for this analysis due to oxygen sensory neurons also having cilia. In total, 1593 genes fit the criteria for further analysis. To normalize the data, we calculated the maximum TPM value a given gene across all cell types, and the TPM for each cell-type was scaled to the proportion of the max. This gave a max of 1 for any given gene for expression. This was carried out for the cell-type specific dataset from Cao et al.[44], as well as the TPM values for genes across 40 clustered neuronal subtypes. Max 1 normalized values for each gene across each cell type was then input into a matrix for t-SNE dimensional reduction and k-means and hierarchical clustering. Multiple iterations of dimensional reduction and clustering were carried out and the location of 77 known cilia genes was compared for each cluster. By excluding two clusters of 443 genes, 73 of 77 known cilia genes were captured using this methodology in the remaining 4 clusters of genes. These 1150 remaining genes were then filtered for genes with a human ortholog and ranked by % of total gene expression in ciliated cell-types vs non-ciliated cell-types for a total of 414 genes.

Visualization of fluorescent proteins in transgenic animals

Fluorescently tagged proteins were visualized by first immobilizing animals using 0.5 µL of 10 mM levamisole and 0.5 µL of 0.1 µm diameter polystyrene microspheres (2.5% w/v suspension) on 7% agarose pads. To assess the subcellular localization of the various fluorescent reporters for both the wild-type and each mutant strain, Z-stacks were captured using an LSM880 laser scanning microscope with Airyscan and Zeiss ZEN 2.3 software.

To normalise the fluorescence levels (Fig. 1E) for PEF-1::GFP, as well as XBX-1::tdTomato (the peak of which is used to define the relative positions of all signals), the intensities of the visible fluorescent signals (spanning from the PCMC to the end of the axoneme) from each fluorescent protein were measured using Zeiss ZEN 2.3 software. All signal intensities were then normalised relative to the peak signal intensity (set at 100) obtained for the fluorescent marker (PEF-1::GFP or XBX-1::tdTomato), and graphed.

Cilium length and morphology measurements

Cilium length and morphology measurements in wild-type and indicated mutant animals were carried out by visualizing GFP reporters expressed in specific ciliated neurons, as described. The length (in µm) of cilia (or ciliary branch in the case of AWB/AWC cilia) was measured by drawing a line longitudinally using the ZEN 2.3 software. The surface areas of the AWB and AWC cilia 'wings' were assessed by measuring at least 14 AWB or AWC 'wing' ciliary branches (both) from each strain, using the ZEN 2.3 software and automatic segmentation based on fluorescence intensity. The aspect ratio (width divided by length) of the AFD finger ciliary compartment was assessed from at least 13 neurons from each strain using the ZEN 2.3 software. Width and length refer to the largest dimensions (in µm) of the structure perpendicular or parallel to the main axis of the dendrite, respectively.

Transmission electron microscopy (TEM)
Animals were prepped and sectioned using standard methods[127]. Images were acquired with an FEI Tecnai G2 Spirit BioTwin transmission electron microscope equipped with a 4 K digital camera. Image processing and analysis was performed using SerialEM and IMOD software[128].

Developmental assays
Gravid adult worms were allowed to lay eggs for 60 min and these egg progenies were grown at 20 °C for 68 h. Then the L4 larvae on each plate were counted and the remaining adults were imaged with Zeiss Axioskop 2 + microscope for evaluating development stage and scored as L4, young adult, mature adult or gravid adult.

Body length measurement
L4-stage worms were placed onto plates with an OP50 bacteria lawn and grown at 20 °C for 48 h. Worms were imaged using Axioskop 2 + microscope, and their body length (length of the midline of worm body) was measured using ImageJ software.

Dye-filling assays
Dye-filling assays were conducted essentially as reported[129], by incubating animals for 30 min in a solution of lipophilic dye (DiI) diluted with M9 buffer 1:1000, followed by recovery (feeding) for 30 min on seeded NGM plates to minimize gut fluorescence. Dye uptake into amphid and phasmid neurons was assessed by fluorescence microscopy. At least 15 staged animals (L4 larvae) were scored for each strain per experiment.

Osmolarity assays
Osmolarity avoidance assays were carried out as reported[129] on unseeded NGM plates by measuring the proportion of adult animals that cross a ring of high osmotic strength (8 M glycerol) within a 10 min timespan. Worms that crossed the barrier were removed from the assay.

Chemotaxis assays
The response to a gradient of NaCl (10 mM to < 1 mM) was based on assays developed by Chang and colleagues[130]. As a control, the *che-3* IFT mutant was used. To establish the chemical gradients on the assay plates, a 10 µL drop of 2.5 M NaCl (pH = 6.0) was placed 15 mm from the edge of the plate at the "attractive spot". A 10 µL drop of ddH_20 was placed diametrically opposite and was considered the "negative control spot". The attractant was allowed to diffuse for 14–16 h at room temperature. To increase the steepness of the chemical gradient, 4 to 4.5 h prior to chemotaxis assay 4 µL attractant was added to the "attractive spot" and 4 µL ddH_20 added to the "negative control spot". Synchronized adult cultures were rinsed off culture plates with ddH20. Before placing animals on assay plates, sodium azide was pipetted onto the "attractive spot" and onto the "negative control spot" to anesthetize animals reaching either spot. Animals were placed in the center of the plate equidistant from the "attractive spot" and the "negative control spot" in a minimal drop of ddH_20. Chemotaxis assays were performed at room temperature for 60 min and assay plates were subsequently placed in a refrigerator (5C) to immobilize animals. The chemotaxis index for an assay plate was calculated as follow:

$$chemotaxis\ index = \frac{animals\ at"\text{attractive spot}"\ - animals\ at"negative\ control\ spot"}{total\ number\ of\ animals\ in\ assay}$$

In the case of a volatile chemoattractant, 10 uL of 1/100 isoamyl alcohol was placed on the attractant spot and 10 µL of 95% ethanol (diluent) was also placed onto the control spot. The behavior of animals was always compared with controls performed on the same day. At least 4 plates were assayed in at least three independent experiments performed on separate days.

CO_2 avoidance analysis
Wild-type, *pef-1*(*gk5346*), *pef-1(G2A)*, *pef-1(C3S)* and *gcy-9*(*tm2816*) mutant adult-stage animals (n = 15) were allowed to lay eggs on a bacterial lawn for 3 h at 20 °C and were then removed. The eggs were hatched and grown for 4 days at the same temperature. After 100 s of placing a plate on a Multi-Worm Tracker (MWT), 10% CO_2 gas was delivered to worms for 4 s and their behavioral (movement) responses were recorded for an additional 146 s. The animal avoidance behaviors (omega-turns and speed) were analyzed and graphed using R software essentially as described previously[131].

Phototosensory avoidance behavior
Phototaxis behavior was analyzed as described previously[85]. Briefly, day 1 adult worms were transferred to NGM plates covered with a thin layer of freshly spread OP50 bacteria ~ 30 min before the test. Worms were tested under a 10 × objective on a fluorescence dissection microscope (Zeiss Discovery). A 2 s light pulse (350 ± 25 nm, 406 mW/mm2, Sola, Lumencor) was delivered to the head of a worm that was slowly moving forward. A positive response was scored if the worm stopped forward movement during the illumination time or 3 s after and initiated a backward movement that lasted at least half a head swing.

Thermosensation
Thermal gradients were generated across an aluminum platform (60 cm x 10 cm × 1.3 cm) attached on either end to two water baths, set to 5℃ and 45℃. Rectangular Petri dishes (86 × 128 mm, Thermo Scientific) containing 20 ml of NGM (2% agar) were placed on an aluminum plate (135 mm × 95 mm, 1 mm) with some water and allowed to equilibrate (typically within 10 min), generating a linear thermal gradient (22℃ – 19℃) across the

agar surface. The gradient was confirmed by measuring the temperature at the agar surface using a small type K probe (Total-Range Thermometer, Fisher Scientific). Animals were reared at 20℃ for all experiments with shifts to 25℃ at least 30 min prior to testing. Briefly, synchronized young adult populations were washed in ddH_2O, then transferred by pipette to the narrow (0.5 cm) starting zone at the center of the plates. Migration was monitored for 60 min since the distribution of animals reaches a steady state in this time window. Time 0 was set as the time when worms began crawling away from the starting zone, typically 2 min after transfer to the assay plate, and experiments were terminated after 60 min by killing worms in situ using chloroform vapor.

The thermotaxis (Ttx) index was calculated as follow:

$$TtxIndex = \frac{\sum_{x=-4}^{+4} x * n_x}{n_{total}}$$

n_x = number of animals in each region (x = -4 ~ +4).

n_{total} = total number of animals.

Statistical analyses

Data distribution was determined by Shapiro–Wilk test. If the data had a normal distribution, the statistical significance was calculated by Tukey's honestly significant difference. If the data was not normally distributed, Kruskal–Wallis test was used for calculation of the p-value. When more than three strains were analyzed, the significance was obtained based on Dunn's Kruskal–Wallis Multiple Comparisons with Holm-Sidak adjustment.

Data availability

Data is provided within the manuscript and a supplementary information file.

Received: 25 April 2024; Accepted: 6 November 2024
Published online: 16 November 2024

References

1. Anvarian, Z., Mykytyn, K., Mukhopadhyay, S., Pedersen, L. B. & Christensen, S. T. Cellular signalling by primary cilia in development, organ function and disease. *Nat Rev Nephrol.* **15**(4), 199–219 (2019).
2. Satir, P. & Christensen, S. T. Overview of structure and function of mammalian cilia. *Annu. Rev. Physiol.* https://doi.org/10.1146/annurev.physiol.69.040705.141236 (2007).
3. Bangs F, Anderson KV. Primary Cilia and Mammalian Hedgehog Signaling. Cold Spring Harb Perspect Biol. 2016
4. Gerdes, J. M., Davis, E. E. & Katsanis, N. The vertebrate primary cilium in development, homeostasis, and disease. *Cell* **137**(1), 32–45 (2009).
5. Garcia, G., Raleigh, D. R. & Reiter, J. F. How the ciliary membrane is organized inside-out to communicate outside-In. *Curr. Biol.* **28**(8), R421–R434 (2018).
6. Nachury, M. V. & Mick, D. U. Establishing and regulating the composition of cilia for signal transduction. *Nat. Rev. Mol. Cell Biol.* **20**(7), 389–405 (2019).
7. Uytingco, C. R., Green, W. W. & Martens, J. R. Olfactory loss and dysfunction in ciliopathies: molecular mechanisms and potential therapies. *Curr. Med. Chem.* **26**(17), 3103–3119 (2019).
8. Chen, H. Y., Kelley, R. A., Li, T. & Swaroop, A. Primary cilia biogenesis and associated retinal ciliopathies. *Semin. Cell Dev. Biol.* https://doi.org/10.1016/j.semcdb.2020.07.013 (2021).
9. Barnes, C. L., Malhotra, H. & Calvert, P. D. Compartmentalization of photoreceptor sensory cilia. *Front Cell Dev. Biol.* https://doi.org/10.3389/fcell.2021.636737 (2021).
10. Vaisse, C., Reiter, J. F. & Berbari, N. F. Cilia and obesity. *Cold Spring Harb. Perspect. Biol.* **9**(7), a028217 (2017).
11. Guemez-Gamboa, A., Coufal, N. G. & Gleeson, J. G. Primary cilia in the developing and mature brain. *Neuron* **82**(3), 511–521 (2014).
12. Baker, K. & Beales, P. L. Making sense of cilia in disease: the human ciliopathies. *Am. J. Med. Genet. C Semin. Med. Genet.* **151C**(4), 281–295 (2009).
13. Reiter, J. F. & Leroux, M. R. Genes and molecular pathways underpinning ciliopathies. *Nat. Rev. Mol. Cell Biol.* **18**(9), 533–547 (2017).
14. Braun, D. A. & Hildebrandt, F. Ciliopathies. *Cold Spring Harb. Perspect. Biol.* **9**(3), a028191 (2017).
15. Mitchison, H. M. & Valente, E. M. Motile and non-motile cilia in human pathology: from function to phenotypes. *J. Pathol.* **241**(2), 294–309 (2017).
16. Chen, H. Y., Welby, E., Li, T. & Swaroop, A. Retinal disease in ciliopathies: Recent advances with a focus on stem cell-based therapies. *Transl. Sci. Rare Dis.* **4**(1–2), 97–115 (2019).
17. Hildebrandt, F., Benzing, T. & Katsanis, N. Ciliopathies. *N. Engl. J. Med.* **364**(16), 1533–1543 (2011).
18 Klena, N. T., Gibbs, B. C. & Lo, C. W. Cilia and ciliopathies in congenital heart disease. *Cold Spring Harb. Perspect Biol.* **9**, 8 (2017).
19. Ishikawa, H. & Marshall, W. F. Ciliogenesis: building the cell's antenna. *Nat. Rev. Mol. Cell Biol.* **12**(4), 222–234 (2011).
20 Vertii, A., Hung, H. F., Hehnly, H. & Doxsey, S. Human basal body basics. *Cilia* https://doi.org/10.1186/s13630-016-0030-8 (2016).
21. Carvalho-Santos, Z., Azimzadeh, J., Pereira-Leal, J. B. & Bettencourt-Dias, M. Evolution: Tracing the origins of centrioles, cilia, and flagella. *J. Cell Biol.* **194**(2), 165–175 (2011).
22. Avidor-Reiss, T. & Leroux, M. R. Shared and distinct mechanisms of compartmentalized and cytosolic ciliogenesis. *Curr. Biol.* **25**(23), R1143–R1150 (2015).
23. Fisch, C. & Dupuis-Williams, P. Ultrastructure of cilia and flagella - back to the future!. *Biol Cell.* **103**(6), 249–270 (2011).
24. Sung, C. H. & Leroux, M. R. The roles of evolutionarily conserved functional modules in cilia-related trafficking. *Nat. Cell Biol.* **15**(12), 1387–1397 (2013).
25 Garcia-Gonzalo, F. R. & Reiter, J. F. Open sesame: how transition fibers and the transition zone control ciliary composition. *Cold Spring Harb. Perspect Biol.* **9**, 2 (2017).
26 Jensen, V. L. & Leroux, M. R. Gates for soluble and membrane proteins, and two trafficking systems (IFT and LIFT), establish a dynamic ciliary signaling compartment. *Curr. Opin. Cell Biol.* **4783**, 91 (2017).
27. Reiter, J. F., Blacque, O. E. & Leroux, M. R. The base of the cilium: roles for transition fibres and the transition zone in ciliary formation, maintenance and compartmentalization. *EMBO Rep.* **13**(7), 608–618 (2012).

28. Silverman, M. A. & Leroux, M. R. Intraflagellar transport and the generation of dynamic, structurally and functionally diverse cilia. *Trends Cell Biol.* **19**(7), 306–316 (2009).
29 McEwen, D. P., Jenkins, P. M. & Martens, J. R. Olfactory cilia: our direct neuronal connection to the external world. *Curr. Top Dev. Biol.* https://doi.org/10.1016/S0070-2153(08)00812-0 (2008).
30. Jenkins, P. M., McEwen, D. P. & Martens, J. R. Olfactory cilia: linking sensory cilia function and human disease. *Chem. Senses.* **34**(5), 451–464 (2009).
31 Mirzadeh, Z. et al. Bi- and uniciliated ependymal cells define continuous floor-plate-derived tanycytic territories. *Nat. Commun.* https://doi.org/10.1038/ncomms13759 (2017).
32. Bujakowska, K. M., Liu, Q. & Pierce, E. A. Photoreceptor cilia and retinal ciliopathies. *Cold Spring Harb. Perspect. Biol.* **9**(10), a028274 (2017).
33 Roepman, R. & Wolfrum, U. Protein networks and complexes in photoreceptor cilia. *Subcell Biochem.* **43209**, 235 (2007).
34 Bae, Y. K. & Barr, M. M. Sensory roles of neuronal cilia: cilia development, morphogenesis, and function in C elegans. *Front Biosci.* **135959**, 5974 (2008).
35 Inglis, P. N., Ou, G., Leroux, M. R. & Scholey, J. M. The sensory cilia of Caenorhabditis elegans. *WormBook* https://doi.org/10.1895/wormbook.1.126.1 (2007).
36. Procko, C. & Shaham, S. Assisted morphogenesis: glial control of dendrite shapes. *Curr. Opin. Cell Biol.* **22**(5), 560–565 (2010).
37. Goodman, M. B. & Sengupta, P. How caenorhabditis elegans senses mechanical stress, temperature, and other physical stimuli. *Genetics.* **212**(1), 25–51 (2019).
38 Bargmann, C. I. Chemosensation in C. elegans. *WormBook.* **1**, 29 (2006).
39 Blacque, O. E. & Sanders, A. A. Compartments within a compartment: what C. elegans can tell us about ciliary subdomain composition, biogenesis, function, and disease. *Organogenesis* **10**(1), 126–137 (2014).
40 Goodman, M. B. & Sengupta, P. The extraordinary AFD thermosensor of C. elegans. *Pflugers Arch.* **470**(5), 839–849 (2018).
41. Andreeva, A. V. & Kutuzov, M. A. PPEF/PP7 protein Ser/Thr phosphatases. *Cell Mol. Life Sci.* **66**(19), 3103–3110 (2009).
42. Ramulu, P. & Nathans, J. Cellular and subcellular localization, N-terminal acylation, and calcium binding of Caenorhabditis elegans protein phosphatase with EF-hands. *J. Biol. Chem.* **276**(27), 25127–25135 (2001).
43 Ferkey, D. M., Sengupta, P. & L'Etoile, N. D. Chemosensory signal transduction in Caenorhabditis elegans. *Genetics.* **217**, 3 (2021).
44. Cao, J. et al. Comprehensive single-cell transcriptional profiling of a multicellular organism. *Science* **357**(6352), 661–667 (2017).
45. Steele, F. & O'Tousa, J. E. Rhodopsin activation causes retinal degeneration in Drosophila rdgC mutant. *Neuron* **4**(6), 883–890 (1990).
46. Steele, F. R., Washburn, T., Rieger, R. & O'Tousa, J. E. Drosophila retinal degeneration C (rdgC) encodes a novel serine/threonine protein phosphatase. *Cell* **69**(4), 669–676 (1992).
47. Vinós, J., Jalink, K., Hardy, R. W., Britt, S. G. & Zuker, C. S. A G protein-coupled receptor phosphatase required for rhodopsin function. *Science* **277**(5326), 687–690 (1997).
48. Arendt, D., Tessmar-Raible, K., Snyman, H., Dorresteijn, A. W. & Wittbrodt, J. Ciliary photoreceptors with a vertebrate-type opsin in an invertebrate brain. *Science* **306**(5697), 869–871 (2004).
49 Gong, J. et al. The C elegans taste receptor homolog LITE-1 Is a photoreceptor. *Cell.* **167**(5), 1252-1263.e10 (2016).
50. Arendt, D. Evolution of eyes and photoreceptor cell types. *Int. J. Dev. Biol.* **47**(7–8), 563–571 (2003).
51. Ramulu, P. et al. Normal light response, photoreceptor integrity, and rhodopsin dephosphorylation in mice lacking both protein phosphatases with EF hands (PPEF-1 and PPEF-2). *Mol. Cell Biol.* **21**(24), 8605–8614 (2001).
52. Taylor, S. R. et al. Molecular topography of an entire nervous system. *Cell* **184**(16), 4329-4347.e23 (2021).
53. Blacque, O. E. et al. Loss of C. elegans BBS-7 and BBS-8 protein function results in cilia defects and compromised intraflagellar transport. *Genes Dev.* **18**(13), 1630–1642 (2004).
54 Resh, M. D. Fatty acylation of proteins: The long and the short of it. *Prog. Lipid Res.* **63120**, 131 (2016).
55 Roy, K. & Marin, E. P. Lipid Modifications in Cilia Biology. *J. Clin. Med.* **8**, 7 (2019).
56. Aicart-Ramos, C., Valero, R. A. & Rodriguez-Crespo, I. Protein palmitoylation and subcellular trafficking. *Biochim. Biophys. Acta.* **1808**(12), 2981–2994 (2011).
57. Jensen, V. L. et al. Formation of the transition zone by Mks5/Rpgrip1L establishes a ciliary zone of exclusion (CIZE) that compartmentalises ciliary signalling proteins and controls PIP2 ciliary abundance. *EMBO J.* **34**(20), 2537–2556 (2015).
58. Li, C. et al. MKS5 and CEP290 dependent assembly pathway of the ciliary transition zone. *PLoS Biol.* **14**(3), e1002416 (2016).
59. Gonçalves, J. & Pelletier, L. The ciliary transition zone: finding the pieces and assembling the gate. *Mol Cells.* **40**(4), 243–253 (2017).
60. Huang, L. et al. TMEM237 is mutated in individuals with a Joubert syndrome related disorder and expands the role of the TMEM family at the ciliary transition zone. *Am. J. Hum. Genet.* **89**(6), 713–730 (2011).
61. Roberson, E. C. et al. TMEM231, mutated in orofaciodigital and Meckel syndromes, organizes the ciliary transition zone. *J. Cell Biol.* **209**(1), 129–142 (2015).
62. Winkelbauer, M. E., Schafer, J. C., Haycraft, C. J., Swoboda, P. & Yoder, B. K. The C elegans homologs of nephrocystin-1 and nephrocystin-4 are cilia transition zone proteins involved in chemosensory perception. *J Cell Sci.* **118**(23), 5575–5587 (2005).
63. Tong, Y. G. & Burglin, T. R. Conditions for dye-filling of sensory neurons in Caenorhabditis elegans. *J Neurosci. Methods.* **188**(1), 58–61 (2010).
64 Inglis, P. N., Blacque, O. E. & Leroux, M. R. Functional genomics of intraflagellar transport-associated proteins in C. elegans. *Methods Cell Biol* https://doi.org/10.1016/S0091-679X(08)93014-4 (2009).
65. Starich, T. A. et al. Mutations affecting the chemosensory neurons of Caenorhabditis elegans. *Genetics* **139**(1), 171–188 (1995).
66. Ou, G. et al. Sensory ciliogenesis in Caenorhabditis elegans: assignment of IFT components into distinct modules based on transport and phenotypic profiles. *Mol. Biol. Cell.* **18**(5), 1554–1569 (2007).
67. O'Halloran, D. M., Hamilton, O. S., Lee, J. I. & Gallegos, M. L'Etoile ND Changes in cGMP levels affect the localization of EGL-4 in AWC in Caenorhabditis elegans. *PloS one* **7**(2), e31614 (2012).
68. Nguyen, P. A., Liou, W., Hall, D. H. & Leroux, M. R. Ciliopathy proteins establish a bipartite signaling compartment in a C. elegans thermosensory neuron. *J Cell Sci.* **127**(24), 5317–5330 (2014).
69. Perkins, L. A., Hedgecock, E. M., Thomson, J. N. & Culotti, J. G. Mutant sensory cilia in the nematode Caenorhabditis elegans. *Dev Biol.* **117**(2), 456–487 (1986).
70 Doroquez, D. B., Berciu, C., Anderson, J. R., Sengupta, P. & Nicastro, D. A high-resolution morphological and ultrastructural map of anterior sensory cilia and glia in Caenorhabditis elegans. *Elife.* **3**, e01948 (2014).
71 Mohan, S., Timbers, T. A., Kennedy, J., Blacque, O. E. & Leroux, M. R. Striated rootlet and nonfilamentous forms of rootletin maintain ciliary function. *Curr. Biol.* https://doi.org/10.1016/j.cub.2013.08.033 (2013).
72. Tucker, M., Sieber, M., Morphew, M. & Han, M. The Caenorhabditis elegans aristaless orthologue, alr-1, is required for maintaining the functional and structural integrity of the amphid sensory organs. *Mol. Biol. Cell.* **16**(10), 4695–4704 (2005).
73 Carrillo, M. A. & Hallem, E. A. Gas Sensing in Nematodes. *Mol. Neurobiol.* https://doi.org/10.1007/s12035-014-8748-z (2014).
74. Jensen, V. L. et al. Role for intraflagellar transport in building a functional transition zone. *EMBO Rep.* **19**, 12 (2018).
75. Shakir, M. A., Fukushige, T., Yasuda, H., Miwa, J. & Siddiqui, S. S. C. elegans osm-3 gene mediating osmotic avoidance behaviour encodes a kinesin-like protein. *Neuroreport.* **4**(7), 891–894 (1993).
76. Hallem, E. A. & Sternberg, P. W. Acute carbon dioxide avoidance in Caenorhabditis elegans. *Proc. Natl. Acad. Sci. U.S.A.* **105**(23), 8038–8043 (2008).

77. Bretscher, A. J. et al. Temperature, oxygen, and salt-sensing neurons in C. elegans are carbon dioxide sensors that control avoidance behavior. *Neuron* **69**(6), 1099–1113 (2011).
78 Carrillo, M. A., Guillermin, M. L., Rengarajan, S., Okubo, R. P. & Hallem, E. A. O2-sensing neurons control CO2 response in C. elegans. *J. Neurosci.* **33**(23), 9675–9683 (2013).
79 Kodama-Namba, E. et al. Cross-modulation of homeostatic responses to temperature, oxygen and carbon dioxide in C. elegans. *PLoS Genet.* **9**(12), e1004011 (2013).
80 Swierczek, N. A., Giles, A. C., Rankin, C. H. & Kerr, R. A. High-throughput behavioral analysis in C. elegans. *Nat Methods.* **8**(7), 592–598 (2011).
81. Hallem, E. A. et al. Receptor-type guanylate cyclase is required for carbon dioxide sensation by Caenorhabditis elegans. *Proc. Natl. Acad. Sci. U. S. A.* **108**(1), 254–259 (2011).
82. Smith, E. S., Martinez-Velazquez, L. & Ringstad, N. A chemoreceptor that detects molecular carbon dioxide. *J. Biol. Chem.* **288**(52), 37071–37081 (2013).
83 Goodman, M. B. et al. Thermotaxis navigation behavior. *WormBook* https://doi.org/10.1895/wormbook.1.168.1 (2014).
84. Komatsu, H., Mori, I., Rhee, J. S., Akaike, N. & Ohshima, Y. Mutations in a cyclic nucleotide-gated channel lead to abnormal thermosensation and chemosensation in C. elegans. *Neuron* **17**(4), 707–718 (1996).
85. Ward, A., Liu, J., Feng, Z. & Xu, X. Z. Light-sensitive neurons and channels mediate phototaxis in C. elegans. *Nat Neurosci.* **11**(8), 916–922 (2008).
86 Liu, J. et al. C. elegans phototransduction requires a G protein-dependent cGMP pathway and a taste receptor homolog. *Nat. Neurosci.* **13**(6), 715–722 (2010).
87. Mills, E., Price, H. P., Johner, A., Emerson, J. E. & Smith, D. F. Kinetoplastid PPEF phosphatases: dual acylated proteins expressed in the endomembrane system of Leishmania. *Mol. Biochem. Parasitol.* **152**(1), 22–34 (2007).
88. Strauch, L., Pfannstiel, J., Huber, A. & Voolstra, O. Solubility and subcellular localization of the three drosophila RDGC phosphatase variants are determined by acylation. *FEBS Lett.* **592**(14), 2403–2413 (2018).
89. Dutcher, S. K. Flagellar assembly in two hundred and fifty easy-to-follow steps. *Trends Genet.* **11**(10), 398–404 (1995).
90. Avidor-Reiss, T. et al. Decoding cilia function: defining specialized genes required for compartmentalized cilia biogenesis. *Cell.* **117**(4), 527–539 (2004).
91. Blacque, O. E. et al. Functional genomics of the cilium, a sensory organelle. *Curr. Biol.* **15**(10), 935–941 (2005).
92. Liu, Q. et al. The proteome of the mouse photoreceptor sensory cilium complex. *Mol. Cell Proteomics.* **6**(8), 1299–1317 (2007).
93. Chen, N. et al. Identification of ciliary and ciliopathy genes in Caenorhabditis elegans through comparative genomics. *Genome Biol.* **7**(12), R126 (2006).
94. Jensen, V. L. et al. Whole-organism developmental expression profiling identifies RAB-28 as a novel ciliary GTPase associated with the BBSome and intraflagellar transport. *PLoS Genet* https://doi.org/10.1371/journal.pgen.1006469 (2016).
95. Laurencon, A. et al. Identification of novel regulatory factor X (RFX) target genes by comparative genomics in Drosophila species. *Genome Biol.* **8**(9), R195 (2007).
96. Li, J. B. et al. Comparative genomics identifies a flagellar and basal body proteome that includes the BBS5 human disease gene. *Cell* **117**(4), 541–552 (2004).
97. Pazour, G. J., Agrin, N., Leszyk, J. & Witman, G. B. Proteomic analysis of a eukaryotic cilium. *J. Cell Biol.* **170**(1), 103–113 (2005).
98. Stolc, V., Samanta, M. P., Tongprasit, W. & Marshall, W. F. Genome-wide transcriptional analysis of flagellar regeneration in Chlamydomonas reinhardtii identifies orthologs of ciliary disease genes. *Proc. Natl. Acad. Sci. U.S.A.* **102**(10), 3703–3707 (2005).
99. Hayes, J. M. et al. Identification of novel ciliogenesis factors using a new in vivo model for mucociliary epithelial development. *Dev. Biol.* **312**(1), 115–130 (2007).
100. Prevo, B., Scholey, J. M. & Peterman, E. J. G. Intraflagellar transport: mechanisms of motor action, cooperation, and cargo delivery. *FEBS J.* **284**(18), 2905–2931 (2017).
101. Wingfield, J. L., Lechtreck, K. F. & Lorentzen, E. Trafficking of ciliary membrane proteins by the intraflagellar transport/BBSome machinery. *Essays Biochem.* **62**(6), 753–763 (2018).
102. Hukema, R. K., Rademakers, S., Dekkers, M. P., Burghoorn, J. & Jansen, G. Antagonistic sensory cues generate gustatory plasticity in Caenorhabditis elegans. *EMBO J.* **25**(2), 312–322 (2006).
103. Suzuki, H. et al. Functional asymmetry in Caenorhabditis elegans taste neurons and its computational role in chemotaxis. *Nature* **454**(7200), 114–117 (2008).
104 Matsuyama, H. J. & Mori, I. 2020 Neural coding of thermal preferences in the nematode Caenorhabditis elegans. *eNeuro.* **7**(3), 0414–0419 (2020).
105 Kimura, K. D., Miyawaki, A., Matsumoto, K. & Mori, I. The C. elegans thermosensory neuron AFD responds to warming. *Curr. Biol.* **14**(14), 1291–1295 (2004).
106. Bretscher, A. J., Busch, K. E. & de Bono, M. A carbon dioxide avoidance behavior is integrated with responses to ambient oxygen and food in Caenorhabditis elegans. *Proc. Natl. Acad. Sci. U.S.A.* **105**(23), 8044–8049 (2008).
107. Dunsenbery, D. B. Video camera-computer tracking of nematode Caenorhabditis elegans to record behavioral responses. *J. Chem. Ecol.* **11**(9), 1239–1247 (1985).
108. Fain, G. L., Hardie, R. & Laughlin, S. B. Phototransduction and the evolution of photoreceptors. *Curr. Biol.* **20**(3), R114–R124 (2010).
109. Voolstra, O. & Huber, A. Ca^{2+} Signaling in drosophila photoreceptor cells. *Adv. Exp. Med. Biol.* **1131857**, 879 (2020).
110. Montell, C. Drosophila visual transduction. *Trends Neurosci.* **35**(6), 356–363 (2012).
111. Jékely, G. Evolution of phototaxis. *Philos. Trans. R Soc. Lond B Biol. Sci.* **364**(1531), 2795–2808 (2009).
112. Byk, T., Bar-Yaacov, M., Doza, Y. N., Minke, B. & Selinger, Z. Regulatory arrestin cycle secures the fidelity and maintenance of the fly photoreceptor cell. *Proc. Natl. Acad. Sci. U. S. A.* **90**(5), 1907–1911 (1993).
113. Lee, S. J. & Montell, C. Regulation of the rhodopsin protein phosphatase, RDGC, through interaction with calmodulin. *Neuron* **32**(6), 1097–1106 (2001).
114. Voolstra, O. et al. The phosphorylation state of the drosophila trp channel modulates the frequency response to oscillating light in vivo. *J. Neurosci.* **37**(15), 4213–4224 (2017).
115. Schou, K. B., Pedersen, L. B. & Christensen, S. T. Ins and outs of GPCR signaling in primary cilia. *EMBO Rep.* **16**(9), 1099–1113 (2015).
116 Kahn-Kirby, A. H. & Bargmann, C. I. TRP channels in C. elegans. *Annu. Rev. Physiol.* https://doi.org/10.1146/annurev.physiol.68.040204.100715 (2006).
117. Kolesnikov, A. V. et al. Dephosphorylation by protein phosphatase 2A regulates visual pigment regeneration and the dark adaptation of mammalian photoreceptors. *Proc. Natl. Acad. Sci. U. S. A.* **114**(45), E9675–E9684 (2017).
118 Kutuzov, M. A. et al. Protein Ser/Thr phosphatases PPEF interact with calmodulin. *Biochem. Biophys. Res. Commun.* **293**(3), 1047–1052 (2002).
119. Chin, D. & Means, A. R. Calmodulin: a prototypical calcium sensor. *Trends Cell Biol.* **10**(8), 322–328 (2000).
120. Sherman, P. M. et al. Identification and characterization of a conserved family of protein serine/threonine phosphatases homologous to Drosophila retinal degeneration C. *Proc. Natl. Acad. Sci. U. S. A.* **94**(21), 11639–11644 (1997).
121 Hardie, R. C. & Juusola, M. Phototransduction in drosophila. *Curr. Opin. Neurobiol.* **3437**, 45 (2015).
122. Brown, B. M., Carlson, B. L., Zhu, X., Lolley, R. N. & Craft, C. M. Light-driven translocation of the protein phosphatase 2A complex regulates light/dark dephosphorylation of phosducin and rhodopsin. *Biochemistry* **41**(46), 13526–13538 (2002).

123. Phua, S. C., Lin, Y. C. & Inoue, T. An intelligent nano-antenna: Primary cilium harnesses TRP channels to decode polymodal stimuli. *Cell Calcium.* **58**(4), 415–422 (2015).
124. Palczewski, K., Hargrave, P. A., McDowell, J. H. & Ingebritsen, T. S. The catalytic subunit of phosphatase 2A dephosphorylates phosphoopsin. *Biochemistry.* **28**(2), 415–419 (1989).
125. Jing, S. & Yi, X. Exome sequencing reveals PPEF2 variant associated with high myopia. *Gene*. **897**, 148091 (2024).
126 Chiang, C. Y. et al. Novel eye genes systematically discovered through an integrated analysis of mouse transcriptomes and phenome. *Comput. Struct. Biotechnol. J.* https://doi.org/10.1016/j.csbj.2019.12.009 (2020).
127. Lundquist, E. A., Reddien, P. W., Hartwieg, E., Horvitz, H. R. & Bargmann, C. I. Three C. elegans Rac proteins and several alternative Rac regulators control axon guidance, cell migration and apoptotic cell phagocytosis. *Development* **128**(22), 4475–4488 (2001).
128. Schorb, M., Haberbosch, I., Hagen, W. J. H., Schwab, Y. & Mastronarde, D. N. Software tools for automated transmission electron microscopy. *Nat. Methods.* **16**(6), 471–477 (2019).
129. Williams, C. L. et al. MKS and NPHP modules cooperate to establish basal body/transition zone membrane associations and ciliary gate function during ciliogenesis. *J. Cell Biol.* **192**(6), 1023–1041 (2011).
130. Chang, S., Johnston, R. J. J., Frokjaer-Jensen, C., Lockery, S. & Hobert, O. MicroRNAs act sequentially and asymmetrically to control chemosensory laterality in the nematode. *Nature* **430**(7001), 785–789 (2004).
131. Park, K. et al. CDKL kinase regulates the length of the ciliary proximal segment. *Curr. Biol.* **31**(11), 2359-2373.e7 (2021).

Acknowledgements

We would like to thank Dr. Donald Moerman (University of British Columbia) and Dr. Piali Sengupta (Brandeis University) for worm strains. This work was funded by the Canadian Institutes of Health Research (CIHR grants MOP-142243 and PJT-156042 to M.R.L.), and NIH grants R35NS105094 to S.S. and R35GM126917 to S.X. Electron microscopy was performed at the Simons Electron Microscopy Center and National Resource for Automated Molecular Microscopy located at the New York Structural Biology Center, and supported by grant SF349247 from the Simons Foundation, NYSTAR, and NIH National Institute of General Medical Sciences grant GM103310. M.R.L. holds a Michael Smith Foundation for Health Research (MSFHR) senior scholar award.

Author contributions

M.R.L., M.B., S.H. and X.Z.S.U., wrote the main manuscript text and prepared figures. M.B., Y.L, K.K., X.Z., C.L., K.P., A.W. contributed data. All authors reviewed the manuscript.

Declarations

Competing interests

The authors declare no competing interests.

Additional information

Supplementary Information The online version contains supplementary material available at https://doi.org/10.1038/s41598-024-79057-z.

Correspondence and requests for materials should be addressed to M.R.L.